CONF-780342--1

THE MECHANISTIC PREDICTION OF TRANSIENT FISSION-GAS RELEASE FROM LWR FUEL

By

J. Rest and S. M. Gehl

MASTER

Prepared for

IAEA Specialists Meeting on
Fuel Element Modeling
Blackpool, United Kingdom
March 13-17, 1978

U of C-AUA-USDOE

ARGONNE NATIONAL LABORATORY, ARGONNE, ILLINOIS

Operated under Contract W-31-109-Eng-38 for the
U. S. DEPARTMENT OF ENERGY

DISCLAIMER

The facilities of Argonne National Laboratory are owned by the United States Government. Under the terms of a contract (W-31-109-Eng-38) between the U. S. Department of Energy, Argonne Universities Association and The University of Chicago, the University employs the staff and operates the Laboratory in accordance with policies and programs formulated, approved and reviewed by the Association.

MEMBERS OF ARGONNE UNIVERSITIES ASSOCIATION

The University of Arizona
Carnegie-Mellon University
Case Western Reserve University
The University of Chicago
University of Cincinnati
Illinois Institute of Technology
University of Illinois
Indiana University
Iowa State University
The University of Iowa
Kansas State University
The University of Kansas
Loyola University
Marquette University
Michigan State University
The University of Michigan
University of Minnesota
University of Missouri
Northwestern University
University of Notre Dame
The Ohio State University
Ohio University
The Pennsylvania State University
Purdue University
Saint Louis University
Southern Illinois University
The University of Texas at Austin
Washington University
Wayne State University
The University of Wisconsin

THE MECHANISTIC PREDICTION OF TRANSIENT FISSION-GAS RELEASE FROM LWR FUEL*

J. Rest and S. M. Gehl

Materials Science Division
ARGONNE NATIONAL LABORATORY
Argonne, Illinois 60439

ABSTRACT

The steady-state and transient gas release and swelling subroutine (GRASS-SST) is a mechanistic computer code for the prediction of fission-gas behavior in UO_2-base fuels. GRASS-SST treats fission-gas release and fuel swelling on an equal basis and simultaneously treats all major mechanisms that influence fission-gas behavior. The GRASS-SST transient analysis has evolved through comparisons of code predictions with the fission-gas release and physical phenomena that occur during reactor operation and transient direct-electrical heating (DEH) testing of irradiated light-water reactor fuel. The GRASS-SST steady-state analysis has undergone verification for end-of-life fission-gas release and intragranular bubble-size distributions. The results of GRASS-SST predictions for transient fission-gas release during DEH tests are in good agreement with experimental data. Comparisons of GRASS-SST predictions of gas release and bubble-size distributions with the results of DEH transient tests indicate that (1) coalescing bubbles do not have sufficient time to grow to equilibrium size during most transient conditions, (2) mobilities of fission-gas bubbles in UO_2 are enhanced during nonequilibrium conditions if the excess pressure in the bubble is sufficient to generate an equivalent stress greater or equal to the yield stress of the surrounding matrix, and

---

*Work supported by the U.S. Nuclear Regulatory Commission.

(3) channel formation on grain surfaces and coalescence of the channels with each other and with the tunnels of gas along the grain edges can contribute to grain-boundary separation and/or the rapid, long-range interconnection of porosity. The phenomena of grain-boundary separation and/or long-range interconnection of porosity provides an important release mechanism for fission gas that has moved out of the grains of irradiated fuel.

THE MECHANISTIC PREDICTION OF TRANSIENT FISSION-GAS RELEASE FROM LWR FUEL*

J. Rest and S. M. Gehl

Materials Science Division
ARGONNE NATIONAL LABORATORY
Argonne, Illinois 60439

I. Introduction

The influence of fission gases on the performance of oxide fuels has been the subject of many investigations over the past twenty years [1]. The inert fission gases produced during irradiation are known to precipitate into bubbles. The bubbles grow as a result of bubble coalescence and diffusion of gas atoms to bubbles. The growing bubbles cause the fuel to swell. Fission gas released from the fuel to the fuel-rod plenum and fuel-cladding gap stresses the cladding, degrades the thermal conductivity of the gap-gas mixture, and thus increases the fuel-rod operating temperatures. Fission-gas behavior during normal operation is fairly well known and is considered in fuel design. The effects of fission gas on the behavior of the fuel are not well known and may be more severe during off-normal conditions than for steady-state irradiations because of increased fuel temperatures. Large stresses on the cladding can lead to cladding rupture, whereas excessive fuel temperatures can result in fuel melting.

The importance of fission-gas behavior in nuclear reactor safety studies stems from two considerations: (a) the possible release of radioactive Kr, Xe, and I isotopes through a breach in the fuel-rod cladding into the environment during postulated accident situations; and (b) the need to determine

---

*Work supported by the U.S. Nuclear Regulatory Commission.

whether a fuel rod may be operated safely after a transient during which gas is released from the oxide pellets without cladding rupture. Although the empirical models used by manufacturers for the prediction of gas release during normal operation are adequate for present-day licensing analyses, considerable uncertainty exists as to the expected gas release during transients [1]. Although many in-reactor experiments have been performed over a range of transient conditions, interpretation of the results is complicated by uncertainties in fuel-temperature measurements that lead to large variances in release fraction [1,2]. In addition, the use of empirical models precludes the possibility of a predictive capability outside the range of conditions used to derive the empirical correlation.

In general, mechanistic models developed over the past twenty years to predict the behavior of fission gases in oxide fuels have enjoyed limited success. They have evolved through the synergistic interplay of mechanisms for fission-gas behavior. As limitations in the predictive capability of the models were discovered additional mechanisms thought to have a dominant effect on fission-gas release and swelling were included. For example, the early Booth model [3] was based on the diffusion of gas atoms in a concentration gradient within a spherical volume to the surface of the sphere where the gas was assumed to be released. Yuill et al. [4] enlarged on the Booth model by including the effects of temperature gradients and by assuming that the gas atoms were released when the gas reached the pellet surface rather than being released from the boundary of an "equivalent" volume. MacEwan and Stevens [5] and Carroll et al. [6] included the effects of gas-atom trapping based on the results of experiments that indicated a decrease in diffusion coefficient with an increase in fission rate and exposure. In the early 1960s observations of fission-gas bubbles in irradiated UO_2 [7] introduced the

possibility that fission-gas release might be controlled by bubble behavior rather than by atomic diffusion. In addition, it was demonstrated that fission-gas bubbles could be destroyed as a result of re-solution of gas atoms from bubbles in an irradiation field [8]. Subsequently, the substantial effect of grain-edge interlinked porosity on gas release and fuel swelling was demonstrated [9,10]. Finally, transient heating tests [11,12] on irradiated fuel have indicated that fission-gas-bubble behavior may have an important effect on the evolution of the fuel microstructure by causing grain-boundary separation. Grain-boundary separation can then provide pathways that permit the trapped fission gas to escape from the fuel.

Any model that attempts a realistic description of fission-gas release and swelling as functions of fuel fabrication variables and a wide range of reactor operating conditions must treat fission-gas release and fuel swelling as coupled phenomena and must include many mechanisms influencing fission-gas behavior. In addition, a mechanistic treatment of fission-gas phenomena includes the potential for a predictive capability outside the range of conditions used for model verification.

The Steady-state and Transient Gas-Release and Swelling Subroutine (GRASS-SST) is a computer program written to predict fission-gas behavior over a wide range of light-water reactor (LWR) conditions. GRASS-SST is based on the GRASS code first reported by Poeppel [13]. GRASS was originally developed for the prediction of fission-gas behavior in Liquid-Metal Fast-Breeder Reactor (LMFBR) fuel during steady-state irradiations, and was designed to be compatible with the LIFE LMFBR fuel-performance code [14,15].

GRASS-SST calculations include the effects of production of gas from fissioning uranium atoms; bubble nucleation; a realistic equation of state for xenon; lattice bubble diffusivities based on experimental observations; bubble diffusion; bubble migration; bubble coalescence; re-solution; temperature and temperature gradients; interlinked porosity; and fission-gas interaction

with structural defects on both the distribution of fission gas within the fuel and the amount of fission gas released from the fuel. GRASS-SST calculates the fission-gas-induced swelling due to, and the fission-gas-bubble-size distributions for, bubbles in the lattice, on grain boundaries, on dislocations, along the grain edges, and the total fission-gas release as a function of time for steady-state and transient conditions. Fission gas released from the fuel reaches the fuel surface by successively diffusing from the grains to grain boundaries and then to the grain edges where the gas percolates out through a network of interconnected tunnels of fission-gas and fabricated porosity.

GRASS-SST has evolved through comparisons of code predictions with the fission-gas releases and physical phenomena that occur during reactor operation and transient Direct-Electrical-Heating (DEH) tests of irradiated LWR fuel. The DEH tests are specifically designed to aid in the development and verification of the transient portion of the GRASS-SST code. The DEH tests have provided two distinctly different types of input. First, in some cases, discrepancies between the predicted and measured gas-release fraction pointed out deficiencies in the existing models. New models were then developed based on independent knowledge or theories of the physical processes involved. The treatment of heating-rate effects on fission-gas-bubble mobility and growth evolved in this way.

Second, additional gas-release mechanisms were directly observed in the DEH tests. The GRASS-SST description of grain-surface channel formation is based on such observations [11,12]. Grain-surface channels can coalesce with each other as well as with the grain-edge tunnels and therefore contribute to intergranular separation and/or cause long-range pore interlinkage. This concept of fission-gas release is in strong contrast to earlier models, many of which are based on the assumption that the gas is released once it encounters a grain boundary.

In the present paper, the DEH test results for a series of power-cooling mismatch (PCM) simulations will be described and compared with the results of in-reactor transients to establish the validity of the DEH technique. The GRASS-SST models based on the experimental results will then be described. Finally, GRASS-SST predictions of fission-gas release will be compared with results obtained from steady-state irradiations and DEH experiments.

2. Transient DEH experiments

2.1. Fuels

The DEH experiments were performed on two fuel types with different irradiation histories. Most of the experiments were performed on commercial pressurized water reactor (PWR) fuel obtained from the H. B. Robinson No. 2 Reactor. Fuel from rods F7 and G6 of assembly B05 were used in the present study. This fuel was irradiated to a peak burnup of 3.14 at.% in two reactor cycles at peak linear heat-generation rates (LHGR) of 22.4 and 17.7 kW/m, respectively [12]. The axial power profiles for the rods contained broad plateaus that extended over the central ∿2.5 m of the 3.7-m fuel regions [16]. The rod-averaged fission-gas release during the Robinson irradiation was ∿0.2% of the amount generated [17]. The low gas release is indicative of low operating temperatures.

During irradiation, the density of the Robinson fuel increased from the as-fabricated value of 92% to a final density of 94% of theoretical. Approximately half of the porosity in the irradiated fuel is in the form of large, roughly spherical pores with diameters in the range 0.03-0.25 mm. These pores, formed during fabrication, were apparently not altered during irradiation. Examples of this type of porosity are visible in the polished plane section through an as-irradiated fuel pellet from the high power region shown in fig. 1. Most of the remaining porosity consists of isolated intergranular pores that are too small to be visible at the magnification of fig. 1. These pores range in size from 0.5 to 2.0 μm and have a specific surface area of 69 mm^2/mm^3. The

fine-scale pores are remnants of the as-fabricated porosity after in-reactor densification. A third class of porosity, consisting of nearly spherical features with diameters between 10 and 50 nm, was also present within the grains and on the grain boundaries of the as-irradiated structure. Because of their small size, these features were assumed to be fission-gas bubbles. Estimates of the density of fission-gas bubbles from replica fractographs gave values of 10^{10} to 10^{11} bubbles/mm^3. For fractional radii $\lesssim$0.7, the grain size (mean linear intercept) increased during irradiation to $\sim$6 μm from an initial value of $\sim$3 μm.

One DEH experiment was performed on a specimen taken from an experimental load-follower rod irradiated in the Saxton PWR. This rod, no. 843, experienced peak LHGRs of $\sim$50 kW/m for short periods during its irradiation [18]. Pronounced axial power peaking also occurred. At the axial level from which the DEH test specimen was obtained, the time-averaged LHGR was $\sim$36 kW/m [18]. The rod-averaged fission-gas release for rod 843 was 8.5%.

A transverse section through rod 843 at $\sim$0.43 m above the rod bottom is shown in fig. 2. This position was slightly above the peak power position. A zone of high density fuel extends from a fractional radius of $\sim$0.60 to the outer pellet radius. The microstructure of this material was apparently almost unaltered during irradiation. For fractional radii $\lesssim$0.60, the grain size was larger (10-12 μm mean linear intercept). Intergranular porosity was present in this central zone. The inner zone is the dark gray region in the center of the section showing in fig. 2. Radial cracks extend inward from the pellet radius to roughly the boundary of the grain-growth region. Most of these cracks end in a large circumferential crack that lies close to the boundary between the inner and outer zones.

The total amounts of fission gas retained in the fuels after irradiation were determined to allow calculations of the fractional releases during DEH transients. The fission-gas retention was determined by collecting and analyzing the gases released when fuel specimens were dissolved in nitric acid. The results of fuel-dissolution experiments on Robinson and Saxton fuel specimens are given in table 1. The data listed for the Saxton fuel correspond to the axial position from which the DEH test specimen was obtained. These values were interpolated from the results of three dissolution experiments at nearby locations.

2.2. The DEH technique

In the DEH technique [19,20], electric current is passed through a stack of pellets in the axial direction. The specimen is cooled by flowing helium. The ohmic heating of the UO_2 and the radial heat loss to the helium coolant produce a radial temperature profile that approximates the profiles obtained for nuclear heating. The electronic control circuitry of the apparatus used for the present experiments is capable of varying the power-input levels and power-ramp rates over wide ranges to simulate the temperature profiles of a variety of nuclear heating conditions. The equipment has the capability for collecting and sampling the fission gas released during transient heating of LWR fuels. The helium-coolant stream passes over the sample and through a series of traps and filters to remove particulate and condensable material before leaving the hot cell. Released fission gases are carried along with the helium stream and collected on activated charcoal traps. Volumetric, chemical, and isotopic analyses of the fission gases are performed after the DEH tests. Details of the experimental methods and specimen-preparation procedures are given in ref. 12.

Transient temperature histories of the DEH tests are calculated with the DEH Transient Temperature Distribution (DEHTTD) code [21]. The transient heat-transfer equation is solved by this code, which accepts measured values of current, voltage, and surface temperature as input and uses expressions taken from the literature for the thermal and electrical conductivities of UO_2.

For use in the present study, a model for the effect of intergranular separations on heat transfer was included in the DEHTTD code. These separations, which are described in the next section, form during transient heating and reduce the effective thermal conductivity of the fuel. In the DEHTTD code, the separations are assumed to form linearly with time, and the reduction in thermal conductivity is assumed to be proportional to the extent of the separations, as measured by their specific surface area. That is, the code uses a thermal-conductivity expression of the form

$$T_K' = (1 - F)T_K ,$$

where T_K' is the effective thermal conductivity, F is the cracking factor (so called because the separations often resemble cracks), and T_K is the temperature-dependent thermal-conductivity expression of Washington [22]. The cracking factor, F, was assumed to equal zero at the start of transient heating and to increase linearly with time to a maximum value, which occurred at maximum power, given by

$$F_{max} = 1.55 \times 10^{-3} S_V^{\alpha P} ,$$

where $S_V^{\alpha P}$ is the posttest value of pore-solid surface area per unit volume in units of mm^{-1}.

2.3. Experimental results

The model development and verification of the transient portion of GRASS-SST are based on the results of 13 PCM-type DEH tests. The experimental conditions, fission-gas release results, calculated temperature history parameters, and quantitative stereology results for these tests are summarized in table 2. The center-line heating rates ranged from 6.0 to 76°C/s. A variety of temperature distributions at the time of maximum power input were produced by selection of the heating rate and test time. Central melt zones were produced in tests 21, 26, 33, and 35. The other transients were terminated prior to melting. The last column in table 2 gives $S_g^{\alpha P}$ as the pore-solid surface area (per gram of fuel) produced during the transient.

The gas-release data were weakly correlated with the DEH energy input, as shown in fig. 3. The dashed lines in this figure indicate the general trend of increasing gas-release fraction with increasing energy input. The datum point for test 31 lies well outside the dashed lines. During test 31, the fuel was operated at a steady-state input of ∿500 W for 1100 s before the transient was applied. The energy deposition during the preheat period was 56.5×10^4 W·s.

Given the wide variation in power ramp rates and maximum power levels, the weak correlation of gas release with energy input is not surprising. However, gas release was strongly correlated with simple representations of the transient temperature history. An example of such a correlation is the plot of % Xe release versus maximum center temperature shown in fig. 4. Gas release increases monotonically as the temperature increases; enhanced gas-release fractions were observed for center-line temperatures in excess of ∿2500°C. Equally strong correlations were obtained when gas release was plotted versus maximum volume-averaged temperature, $\overline{T}_{max}$, or maximum volume-averaged temperature gradient, $(\overline{dT/dR})_{max}$ [11,12]. Gas release was not

correlated strongly with "time-at-temperature" terms such as the time integral of center-line temperature [11,12].

The relatively high gas-release fractions of the DEH-tested specimens suggest the existence of pathways that allow some or all of the gas which reaches the grain boundaries to escape. Examination of the posttest microstructure confirmed the presence of such pathways and indicated the processes responsible for their formation.

The most readily apparent difference between the pre- and posttest fuel structures is the presence of patterns of intergranular separations in the latter. Intergranular separations are present in the unmelted regions of specimens in which central melting occurred and in some of the specimens in which no melting occurred. Examples of the various morphologies identified as directional and nondirectional intergranular separations are shown in fig. 5. The initial stages in the formation of directional and nondirectional patterns of intergranular separations are shown in figs. 5A and 5B, respectively. These separations are crack-like in appearance. The patterns of intergranular separation are nearly fully developed in figs. 5C and 5D. Note that, for both directional and nondirectional patterns, almost every grain is adjacent to a separation, and the separations are interlinked over long distances through the structure. Examples of varying degrees of development of both classes of intergranular separation are present in a single test specimen. In some cases, as shown in fig. 5E, wide variations in the amount of directionality occurred over distances of ∿100 μm. For individual test specimens, an appreciable degree of directionality was present in ∿40% of the area that showed intergranular separations. Directional separations tended to be oriented perpendicular to the pellet radius. However, the local orientation direction was influenced by the presence of stress concentrators, such as large pores and cracks, and near contact points between pellet fragments.

The density of intergranular separations also increased in the vicinity of sources of stress concentration.

Varying amounts of plastic deformation are associated with the grains adjacent to the separations. This effect is most evident in the hottest unmelted fuel. An example of this type of plastic flow is shown in fig. 5E. The characteristics exhibited in figs. 5A-E indicate that mechanical stresses are at least partly responsible for the formation of the intergranular separations.

A final example of a form of intergranular separation, shown in fig. 5F, was present in fuel that was heated to temperatures close to the melting point. These separations occupy grain boundaries of all orientations with equal frequency. The rounded outline of these features contrasts with the sharper edges and crack-like appearance of the separations shown in fig. 5A-E. The structure shown in fig. 5F is characteristic of high-temperature grain-boundary swelling.

Evidence that fission-gas effects were, in part, responsible for the formation of the separations was obtained by examining the posttest microstructures in the scanning electron microscope (SEM). Specimens were prepared by fracturing DEH-tested specimens at room temperature. A series of micrographs along a radial traverse of the specimen from test 24 are shown in fig. 6. At the outermost radial positions (figs. 6A and B), intergranular fracture predominated. The grain surfaces are covered with fission-gas bubbles that range in size from the limit of resolution ($\sim$35 nm) to $\sim$50 nm. Where transgranular fracture occurred, no bubbles are visible. A marked increase in bubble size and density (values of $\sim 10^{13}$ bubbles/mm^3 were determined for the area in fig. 6A) has occurred over the as-irradiated microstructures. The average bubble size increases toward the center of the pellet, i.e., where

transient temperatures were higher, as shown in figs. 6C and D. When the bubbles reach ~0.2 μm in diameter, additional bubble coalescence results in the formation of sinuous grain-surface channels (figs. 6C-E). Grain-boundary-channel formation and bubble growth appear to proceed at different rates on individual grain faces, even for faces on the same grain. The arrow in fig. 6F indicates a grain face on which the channels have coalesced to form a nearly complete separation between two adjacent grains. More extensive grain-boundary separation has occurred at the location shown in fig. 6G, and the predominant fracture mode has changed to transgranular. Note that, in addition to the intergranular separations, intragranular bubbles with diameters of 0.1 to 0.3 μm are present. This sequence of micrographs shows how intergranular separations may be formed by a mechanism that involves growth and coalescence of fission-gas bubbles.

The extent of the intergranular separations can be quantitatively characterized by measuring, with quantitative stereology techniques, the pore volume fraction, V_V^P, and pore-solid surface area, $S_V^{\alpha P}$, as functions of radial position. The measurements were performed on optical micrographs and included features $\gtrsim$0.5 μm in size. If pretest values of V_V^P and $S_V^{\alpha P}$ are also known, the volume increase (i.e. swelling) and the new pore-solid surface area produced during the transient can be calculated.

The relationships between gas release and the transient microstructural changes are shown in figs. 7 and 8. Approximately 2% gas release was observed without any microstructural change. For tests in which swelling was $\lesssim$18%, an approximately linear increase in gas release with swelling was observed. For larger swelling values, the percentage gas release increased more rapidly as the swelling increased. The slope change in the % Xe release versus % swelling curve is believed to be the result of the rapid interlinkage of the

intergranular porosity when the pore-volume fraction reaches a critical value. (The term "intergranular porosity," as used in the balance of the present paper, collectively signifies the intergranular bubbles, channels on grain faces and edges, and planar separations observed in the posttest examinations.) The interlinked porosity allows fission gas on grain edges and boundaries to escape. For swelling below the critical value, gas release is believed to occur mainly by diffusional mechanisms. This explanation is consistent with studies of percolation probabilities, in which extensive long-range interconnection of a second phase in a matrix is predicted if the volume fraction of the second phase exceeds a critical value [9,23-25]. Interconnection of the second-phase particles is negligible for volume fractions less than the critical value. Critical volume fractions of 0.07 [9], 0.17 [23], 0.20 [24], and 0.36 [25] have been reported in the literature. In these studies, the critical volume fractions were observed to be functions of the size distribution and the shape of the second-phase particles. Fig. 7 suggests that the critical volume fraction for the interconnection of the intergranular porosity is $\sim$0.18, which is within the range of reported values.

As shown in fig. 8, the use of $S_g^{\alpha P}$ as a measure of the development of intergranular separations yields a result similar to that observed in fig. 7. That is, enhanced gas release occurs for surface-area values $\gtrsim$250 cm^2/g.

The high gas releases during DEH testing, the microstructures observed in transient-tested fuel, and the correlation of gas release and microstructural change indicate that the mechanisms responsible for the formation of the intergranular porosity can operate in series with intragranular bubble diffusion to transport fission gases from the grain interiors to the pellet surface. Therefore, an understanding of the processes involved in the formation of the grain-surface and edge channels and planar intergranular separations is

important for the mechanistic modeling of transient fission-gas release. Preliminary conclusions about these processes can be made from further interpretation of the posttest microstructures.

The series of micrographs in fig. 6 indicates that intergranular separations can form by the diffusion-controlled processes of growth and coalescence of fission-gas bubbles. However, crack-like separations are present at radial positions where the predominant features on the grain surfaces are isolated fission-gas bubbles. That is, the gradual processes of bubble growth and coalescence can be interrupted by the more rapid process of crack propagation.

The stresses responsible for cracking are the result of the applied axial load, differential thermal expansion, and the pressurization of intergranular fission-gas bubbles. The intergranular propagation of the cracks is partly due to the reduction in grain-grain contact area by the intergranular bubbles. Crack propagation is accompanied by varying amounts of plastic flow in the adjacent grains; the amount of plastic flow depends upon the local temperature. For temperatures close to the melting point, stresses are relieved by plastic flow without mechanical cracking, and bubble and channel coalescence are largely responsible for the observed intergranular separations.

The passage of a crack front through a given grain-grain contact can only result in gas release if the gas on that surface has not been vented by the interlinkage of the grain-surface channels to an edge tunnel or preexisting crack that reaches the external surface. This situation suggests a possible analytic treatment in which gas release is viewed as a stochastic process determined by the probabilities of channel interlinkage and crack propagation on every grain surface in the system. The calculational requirements for such an analysis would obviously be quite large. In the GRASS-SST treatment, which will be described in section 4.3, the probabilities for intergranular

separation by bubble growth and coalescence are characterized by a swelling parameter. Stabilized, long-range interlinkage is assumed to occur when local fuel swelling exceeds a critical value. This model is in qualitative agreement with the empirical result of enhanced gas release for fuel swelling above a critical level (see fig. 7).

3. Correlation of nuclear and electrical heating

As a check on the capability of the DEH technique to simulate in-reactor transient conditions, the behavior of the Saxton fuel during a nuclear-heated transient in the power-burst facility (PBF) [26] was compared with that of the Saxton and Robinson fuels during DEH testing. A detailed discussion of the results of this study is beyond the scope of the present paper. However, a brief summary of the principal findings will be given.

Planar intergranular separations of the type shown in fig. 5 were observed on both DEH and PBF-tested Saxton fuel specimens. Nondirectional separations predominated in the Saxton fuel, although directionality did occur in the vicinity of preexisting cracks. For positions near cracks, a marked similarity was noted for the separations in both the transient-tested Saxton and Robinson fuels, as shown in fig. 9. The SEM examination revealed isolated fission-gas bubbles, sinuous tunnels, and planar separations on the grain surfaces of both DEH- and PBF-tested fuels, as shown in fig. 10. The resintering of grain-surface channels was observed in the PBF-tested fuel but not in DEH-tested materials. This difference is almost certainly due to the differences in the transient thermal histories and not to the heating method.

Fuel from just above the film-boiling boundary of the PBF test rod released ~50% of the available fission gas. This value is in the range of fission-gas releases observed for the DEH-tested Robinson fuel. The smaller release fraction during DEH testing of the Saxton fuel (16%) is due to the differences in temperature history for the DEH and PBF transients.

The microstructure comparisons and the gas-release results for the nuclear and electrically heated transients demonstrate that the same mechanisms act to allow fission-gas transport from the grain boundaries to the pellet exteriors. Therefore, the DEH tests can be used to simulate fission-gas behavior during in-reactor transients.

4. Models for fission-gas behavior during transient conditions

4.1. Rate of growth of coalescing bubbles during transient conditions

During steady-state conditions, it is reasonable to assume that, when two fission-gas bubbles coalesce, the noninstantaneous rate of growth of the resultant bubble to equilibrium size can be treated as instantaneous [27]. However, in a transient analysis, this assumption breaks down, and the noninstantaneous rate of growth of coalescing bubbles must be included. The need for a GRASS-SST model that describes the limited rate of growth of coalescing bubbles became apparent when GRASS-SST-calculated bubble-size distributions for DEH test conditions were compared with qualitative experimental observations. The code predicted similar end-of-test bubble distributions in the lattice and on the grain boundaries. However, the observed intragranular bubble densities were much lower than predicted. A similar conclusion concerning the need to include the effects of nonequilibrium coalescing bubbles in the analysis of fission-gas behavior during transient conditions was reported in a comparison of fission-gas release and swelling (FRAS) code predictions with DEH tests on irradiated mixed-oxide fuel [28].

In general, when two bubbles initiate coalescence, a strain field is generated in the lattice around the growing bubble. Initially, bubble coalescence is a volume-conserving process, subsequently, vacancies that move under the influence of the strain field migrate to the bubble, which results in an increase in the bubble volume. As vacancies enter the growing bubble, the strain field gradually relaxes and vanishes (to first order) when the bubble has reached its equilibrium size. A bubble-relaxation time, τ_i, can be defined

such that, at a time $t = \tau_i$ after the initiation of bubble coalescence, the resultant bubble has approached a stable configuration by an amount 1-1/e. A precise determination of τ_i is not within the scope of the GRASS-SST calculations at this time. However, an estimate of τ_i can be obtained from a consideration of lattice-vacancy thermodynamics. The rate equations for the bubble radii and the lattice vacancy concentration will be described to illustrate the approximations involved in estimating τ_i. Let r_i be the sum of the radii of the coalescing bubbles. If primary creep is neglected, the rate of growth of r_i is given by [27,29].

$$\frac{dr_i}{dt} = \frac{D_v}{r_i}\left[c_v - c_v^e \exp(-P_i^{ex}\Omega/kT)\right]. \tag{1}$$

In eq. (1), c_v^e is the fractional equilibrium vacancy concentration given by

$$c_v^e = \exp(-E_v^f/kT) \ , \tag{2}$$

D_v is the vacancy diffusion coefficient given by

$$D_v = D_v^o \exp(-E_v^m/kT) \ , \tag{3}$$

where E_v^f and E_v^m are the vacancy formation and migration energies, respectively, D_v^o is a preexponential factor, and Ω is the atomic volume. P_i^{ex} is the excess internal gas pressure for each bubble of radius r_i given by

$$P_i^{ex} = P_i^g\ (T) - \frac{2\gamma}{r_i} \ , \tag{4}$$

where γ is the effective surface tension, and P_i^g is the gas pressure within a bubble of radius r_i at temperature T. The explicit rate equation for $c_v(T)$ is given by [29]

$$\frac{dc_v}{dt} = -4\pi D_v c_v \sum_{i=1}^{N} r_i C_i + 4\pi D_v c_v^e \sum_{i=1}^{N} r_i C_i \exp(-P_i^{ex}\,\Omega/kT)$$

$$+ \frac{12\sqrt{\pi}}{d} D_v \left[\sum_{i=1}^{N} r_i C_i\right]^{1/2} (c_v^e - c_v) \,, \qquad (5)$$

where C_i is the concentration of bubbles of radius r_i, and d is the grain diameter.

To determine the variation of P_i^{ex}, it is necessary to solve the simultaneous rate equations (1) and (5) for $r_i(t)$ and $c_v(t)$. Obviously the solution of eqs. (1) and (5) can only be obtained numerically. However, the dimensional form of the two contributions to $\dot{c}_v$ and the term in $\dot{r}_i$ suggests three relaxation times [29]: one for the vacancy concentration where the vacancies are supplied by bubbles, one for the vacancy concentration where the vacancies are supplied by grain boundaries, and one for the growth of bubbles given by

$$\tau_i^B = \frac{r_i^2}{D_v c_v^e} \,. \qquad (6)$$

In the following discussion, we shall assume that the rate of growth of non-equilibrium bubbles can be qualitatively characterized by eq. (6).

Instead of directly calculating the individual fission-gas bubble behavior, GRASS-SST groups the continuum of bubble sizes into a relatively small number of bubble-size classes with each size class, i, characterized by an average bubble radius, r_i. The basic GRASS-SST calculation [30] is for the rate at which bubbles grow from the i to the i + 1 size class. The motivation for treating the problem from this level is that much less computer time is required. The effect of a limited rate of growth of coalescing bubbles on the GRASS-SST calculation is a reduction in the rate at which bubbles grow from the i into the i + 1 size class by the amount

$$[1 - (1 - \kappa) \exp(-\Delta t/\tau_i^B)] \ . \qquad (7)$$

Here Δt is the code time step (i.e. the fuel temperatures and stresses are assumed constant during Δt), and κ ($0 \leq \kappa \leq 1$) corresponds to the bubble-class transfer rate that would exist in the total absence of point-defect motion. Eq. (7) is used for both intra- and intergranular fission-gas-bubble coalescence. However, one would expect that, because of enhanced grain-boundary-vacancy diffusion, the grain-boundary-bubble relaxation times would, in general, be smaller than the lattice-bubble relaxation times.

4.2. Gas-channel formation on grain boundaries

The SEM examinations of DEH-tested fuel, described in section 2.3, revealed the development of sinuous channels on the grain faces after a saturation density of grain-boundary fission gas has been attained. These face channels link up and extend to the grain-edge channels, thus enhancing the release of the gas from the grains.

The GRASS-SST model for grain-boundary saturation by fission-gas bubbles is based on the fact that the grain-boundary area occupied by fission-gas bubbles is nearly independent of the bubble-size distribution (i.e. the bubble-surface area is conserved after bubble coalescence). If the gas is assumed to occupy equal, close-packed, touching bubbles, then the maximum areal coverage per unit area of grain boundary is $A^* = 0.907$. Since the bubble size does not affect the atom areal density, the areal coverage by the fission gas is approximately equal to the coverage by a single bubble of radius r_{max}, which is formed by the coalescence of all the gas on the grain face. The assumption that the bubble-surface area is conserved after bubble coalescence leads directly to an expression for r_{max} in terms of the total number of bubbles on the boundary; i.e.

$$r_{max} = r_i \sqrt{N_i} \ , \tag{8}$$

where all bubbles on the grain face are assumed to have radius r_i, and N_i is the total number of bubbles. The condition for grain-boundary saturation by fission gas is then given by

$$\pi r_{max}^2 = \frac{4}{3} \pi a^3 A^* \frac{S_v^{\alpha\alpha}}{14} \ , \tag{9}$$

where an approximate tetrakaidecahedral (14-sided) lattice geometry has been assumed. In eq. (9), a is the grain radius and $S_v^{\alpha\alpha}$ is the grain-boundary area per unit volume. Combining eqs. (8) and (9) leads to an expression for $N_A^{sat}(i)$, the minimum number of gas bubbles with radius r_i per unit area of grain boundary required for saturation

$$N_A^{sat}(i) = \frac{0.395 \ A^*}{14\pi r_i^2} = \frac{0.008}{r_i^2} \ , \tag{10}$$

where $S_v^{\alpha\alpha} = 1.185/a$. For example, the minimum number of 500-Å-dia (5×10^{-5}-mm-dia) bubbles per unit area of grain boundary required for saturation is

$$N_A^{sat}(500) = \frac{0.008}{r_{500}^2} = 1.3 \times 10^7 \text{ bubbles/mm}^2 \ . \tag{11}$$

This result is in reasonable agreement with the measured 500-Å (5×10^{-5}-mm) grain-boundary bubble-saturation density of $2.2\text{-}4.2 \times 10^7/\text{mm}^2$ [31].

4.3. Fission gas along the grain edges

The GRASS-SST calculation [30] for the diffusion of fission-gas atoms from the grain boundaries to the grain edges is based on a model by Fisher [32] for diffusion in an isotropic slab. Fission gas that has migrated from the UO_2 grain surfaces to the grain edges remains trapped at the edges, unless a path exists through which the gas can escape from the fuel.

In the GRASS-SST treatment [30] of interlinked grain-edge porosity, which is statistical in nature, the degree of pore interlinkage along the grain edges is a function of both the grain and pore-size distributions. The model, which is based on the mathematical theory of percolation [33], utilizes the concept of an arbitrary distribution of sites with randomly distributed bonds or links that join pairs of sites. As applied to nuclear fuels, the sites are represented by intergranular pores; a bond is formed when two adjacent pores become connected. The gas released from a section of fuel is determined by the amount of gas that reaches the pores multiplied by the pore-interlinkage fraction; the remaining gas contributes to grain-edge swelling.

In contrast to the experimental results described in section 2.3, the above formalism for calculating the evolution of interconnected porosity does not predict that a rapid increase in long-range porosity interconnection will occur after a critical value of swelling due to fission-gas bubbles has been reached. The reasons for this deficiency are (a) the geometry assumed in the above model does not correspond to observations of DEH- and PBF-tested fuel, (b) GRASS-SST does not include a realistic calculation of the pore-size distribution (pores in which the internal gas pressure is less than the surface-tension-induced pressure), and (c) material properties used in the GRASS-SST calculation of the pore-size distribution are experimentally almost inaccessible.

Thus, to provide a more realistic calculation of the pore-interlinkage fraction, the above model is supplemented by the additional criterion

$$\text{pore-interlinkage fraction} = 1.0 , \qquad \text{if } B_v > B_{vcrit} , \tag{12}$$

where B_v is the calculated volume strain due to fission-gas bubbles, and B_{vcrit} (0.07) is the critical gas-bubble volume fraction above which extensive

long-range interconnection of the grain-edge tunnels is assumed to take place. Turnbull and Tucker [9] observed that, in nontransient-tested UO_2, interlinked grain-edge tunnels were stable when the volume fraction was >0.07. The critical value for tunnel interlinkage in GRASS-SST is taken from their work.

It is recognized that intergranular crack propagation has the potential to release fission gas that would otherwise be trapped on grain surfaces and edges. The DEH tests indicate the likelihood of gas release by this mechanism. However, the magnitude of the effect is unknown.

At the present stage of development, GRASS-SST does not contain models for the formation and interlinkage of the planar intergranular separations observed in DEH-tested fuel, e.g. see fig. 5. In particular, the contribution of these separations to the total swelling does not appear in the calculated value of B_v. As a result, B_{vcrit} is smaller than the critical volume fraction obtained experimentally (see section 2.3).

4.4. The effect of transient heating on intragranular fission-gas bubbles

Analyses with GRASS-SST for steady-state conditions coupled with experimentally determined fission-gas release during DEH tests (see section 2.3) indicate that large quantities of gas are being transported out of the UO_2 grains during transient heating. This release of fission gas from the grains is much greater than can be explained by means of empirical steady-state diffusivities [30]. In addition, analyses for transient-heating conditions indicate that GRASS-SST can account for the rapid diffusion of fission gas out of the UO_2 grains during DEH tests if the high-temperature bubble mobilities are enhanced due to an increased rate of atom attachment to and detachment from the bubble surface. The physical basis behind this approach is as follows. During equilibrium conditions, the bubbles may be faceted, and the rate of motion of a faceted bubble is determined by the frequency of nucleation

of steps instead of the time required for atoms to move from a step on one side of a bubble to a step on the other side (i.e. the atom attachment and detachment rate is slower than predicted by surface diffusion) [34-38]. However, if the atom attachment and detachment rate increased during transient conditions, higher bubble diffusivities would result.

Recrystallization and dislocation sweeping are other phenomena that could, in principle, result in an enhanced release of fission gas from the grains to the grain boundaries during transient-heating conditions. Observations of the DEH-tested pellets reveal no evidence of UO_2 recrystallization. GRASS-SST analyses indicate that a rapid diffusion of fission-gas bubbles ($\sim$100 Å in diameter) as well as gas atoms occurs during the DEH transient heating. Dislocation sweeping could conceivably move fission-gas atoms from the grains to the grain boundaries but is unlikely to have much effect on fission-gas bubbles; the bubbles would act as pinning sites and retard the motion of dislocations. On the other hand, a rapid increase in the atom attachment and detachment rate would lead to increased bubble mobility for small as well as large bubbles.

4.5. The mobility of overpressurized fission-gas bubbles

It has been shown that bubbles intersected by dislocations have higher diffusivities than bubbles in a perfect lattice [39]. The bubble diffusivities were satisfactorily described by a rate-controlling nucleation mechanism, in which ledges introduced into the bubble surface by the dislocation rotated about the dislocation, causing the bubble to migrate. Since dislocations may extend to the grain surfaces, they can serve as channels that facilitate the migration of the bubbles out of the grains to the grain boundaries. During steady-state heating, the dislocation density is relatively small, and the effective diffusivites of the intragranular bubbles would not be expected to be appreciably altered.

However, during transient heating, differential thermal expansion and external loads can increase dislocation densities. The stress field around

overpressurized bubbles can lead to additional increases in the dislocation density near the bubble. Overpressurization is due to a lack of vacancies in a lattice that is not in thermodynamic equilibrium. If the overpressure in a bubble results in an equivalent stress that exceeds the yield strength of the UO_2, then plastic deformation of the material around the bubble will result. As the bubble surface intersects the resultant dislocations, ledges will be produced that can facilitate atom attachment and detachment.

Since plastic deformation of the UO_2 due to an overpressurized bubble is expected to result in a high density of dislocations around the bubble surface, the diffusivity of such a bubble would be expected to increase quite rapidly. In effect, bubble diffusion would depend more on the time required for atoms to move from a step on one side of a bubble to a step on the other (i.e. surface diffusion) than on the frequency of nucleation of steps.

As the lattice approaches thermodynamic equilibrium, the bubbles will expand at a faster rate as a result of the availability of lattice vacancies and will lose their overpressurization. When the material around a bubble is no longer undergoing plastic deformation, the dislocations will quickly anneal out. Under these conditions, bubble mobility will be quickly reduced as the diffusion of the bubbles becomes once again dominated by the frequency of step nucleation.

4.6. A model for the diffusion of overpressurized fission-gas bubbles

In an attempt to quantify the ideas presented in section 4.5, consider the excess internal gas pressure in a bubble of radius r_i that is given by

$$P_i^{ex} = P_i^g\,(T) - \frac{2\gamma}{r_i}\,, \tag{13}$$

where γ is the effective surface tension, and

$$P_i^g(T) = 3n_i kT/(4\pi r_i^3 - 3b_v n_i) \tag{14}$$

is the gas pressure within the bubble at temperature T. Eq. (14) is a rearrangement of the Van der Waals equation; $b_v = 8.3 \times 10^{-23}$ is Van der Waals constant for xenon/krypton, k is the Boltzmann constant, and n_i is the number of gas atoms in the bubble of radius r_i. P_i^{ex} is a measure of the resultant pressure in the matrix, which vanishes under the initial equilibrium conditions. In eq. (13), the effect of external stresses has been neglected. Consider a time interval, Δt seconds, of the transient during which the fuel temperatures are increasing at a rate dT/dt (°C/s). During this time, bubble coalescence and re-solution are assumed not to occur and n_i is constant and given by the initial equilibrium conditions

$$n_i = \frac{8}{3} \pi \gamma r_i^3 / (k T_1 r_i + 2\gamma b_v) \ , \tag{15}$$

where T_1 is the temperature at the beginning of the time interval Δt.

First consider the case where the bubble radius, r_i, is constant over the time interval Δt. The time τ_i^y required for the bubble to obtain an excess pressure sufficient to generate an equivalent stress equal to the yield stress, σ_y, of the surrounding matrix is, using eqs. (13) and (14), given by

$$\tau_i^y = \left[\frac{\left(\frac{2\gamma}{r_i} + \frac{2\sigma_y}{3} \right) \left(4\pi r_i^3 - 3 b_v n_i \right)}{3 n_i k} - T_1 \right] \Bigg/ \frac{dT}{dt} \ , \tag{16}$$

where $\sigma_y = \sigma_y(T)$ is used to emphasize that σ_y is a strong function of the fuel temperature. Eq. (16) does not take into account the situation in which the bubble may be overpressurized prior to the beginning of the time interval Δt. If the bubble was initially in an overpressurized state, then eq. (16) would overestimate the time required for the equivalent stress generated by the overpressurized bubble to become equal to σ_y. On the other hand, if appreciable bubble relaxation occurs during time τ_i^y (i.e. r_i increases), then eq. (16) would underestimate the time required for the equivalent stress generated by

the overpressurized bubble to become equal to σ_y.

A rigorous approach to the calculation of the excess internal gas pressure for each bubble of radius r_i, where i varies over the limits of the bubble size distribution, requires the numerical solution of a large set of coupled partial differential equations for the rate of change of bubble radii and the rate of change of the lattice-vacancy concentration, c_v [29]. Because of code running time requirements, this approach is outside the scope of GRASS-SST. However, a phenomenological approach to the problem of bubble overpressurization can be formulated by evaluating τ_i^y as given by eq. (16) with respect to the bubble-relaxation time, τ_i^B.

Let α_i, $0 \leq \alpha_i \leq 1$, characterize the degree of nonequilibrium in the lattice surrounding a bubble of radius r_i; the larger α_i the farther the system is from an equilibrium configuration. The change in α_i can be written in terms of α_i and times τ_i^y and τ_i^B [i.e. see eqs. (6) and (16)] as

$$d\alpha_i = (1 - \alpha_i)\, d(\tau_i^B/\tau_i^y) \quad . \tag{17}$$

Thus, as τ_i^y decreases and τ_i^B increases, the system departs more from its equilibrium configuration. Conversely, as τ_i^y increases and τ_i^B decreases, the system approaches equilibrium. Solving eq. (17) for α_i gives

$$\alpha_i = 1.0 - \exp(-\tau_i^B/\tau_i^y) \quad . \tag{18}$$

The problem that remains is to relate α_i to the bubble diffusivity. This can be accomplished by considering the limits of the bubble diffusivities used in GRASS-SST. During steady-state conditions (i.e. $\alpha_i << 1$), GRASS-SST uses empirical intragranular diffusivities given by [30]

$$D_i^{\ell} = 2.1 \times 10^{-4} \exp(-91{,}000/kT)(r_1/r_i)^{1.62} \quad . \tag{19}$$

Eq. (19) is limited by constraints of compatibility with theoretical treatments of bubble mobility by surface diffusion. The diffusivity of a bubble moving by surface diffusion is given by

$$D_i^s = 2.42 \times 10^{-25} \exp(-108{,}000/kT)/r_i^4 . \qquad (20)$$

Based on the discussions above the bubble diffusivities during transient heating conditions should be given by eq. (20) as $\alpha \rightarrow 1$. Thus, using eqs. (19) and (20), the fission-gas-bubble diffusivities can be expressed in terms of the equilibrium parameter, α_i, as

$$D_i = \frac{6.732 \times 10^{-11} \exp[-(91{,}000 + 17{,}000\ \alpha_i)/kT]}{(4084\ r_i)^{(1.62+2.38\alpha_i)}} , \qquad (21)$$

where r_1 of eq. (19) is assumed to have the value of 0.24×10^{-7} cm. When $\alpha_i \rightarrow 0$ eq. (21) $\rightarrow$ eq. (19), and when $\alpha_i \rightarrow 1$ Eq. (21) $\rightarrow$ eq. (20). For intermediate values of α_i, the diffusivities given by eq. (21) lie in between those given by eq. (19) as a lower limit and those given by eq. (20) as an upper limit.

To use eq. (21), the UO_2 yield stress, σ_y, in eq. (19) must be determined. In general, σ_y is a complex function of fuel temperature, strain rate, and microstructure (e.g. UO_2 grain size). Experiments designed to measure the UO_2 yield stress under steady-state and transient in-reactor conditions are difficult to perform and adequate data are lacking. The UO_2 yield stress used in the calculation of gas-bubble diffusivities, as given by eq. (21), has been determined based on the data of Roberts [40]. Roberts conducted conventional load versus deflection, strain-rate change, and stress-relaxation tests on UO_2-20 wt% PuO_2 specimens in the strain-rate range from 0.1 to 0.4 h^{-1} and in the temperature range from 1500 to 1800 C. The specimens, prepared from mechanically blended

powders with grain sizes from 2 to 14.5 μm, were deformed in four-point bending in a high-temperature, inert-atmosphere furnace. The most significant observations from these experiments are the strong temperature dependence of the flow stress (flow stress decreases as the temperature increases) and the increase in flow stress with an increase in grain size (in these experiments the flow stress corresponds to the proportional elastic limit stress).

An analytical expression for the yield stress as a function of the temperature and grain size was obtained from Roberts' data by quadratic regression analysis. Explicitly, for σ_y (in dynes/cm^2)

$$\sigma_y = 9.8 \times 10^5 \exp(a_0 + a_1/T + a_2/T^2) \ , \qquad (22)$$

where

$$a_0 = -179.1 + 7.0d + 0.2d^2 \ ,$$

$$a_1 = 6.5 \times 10^5 - 2.3 \times 10^4 d - 8.6 \times 10^2 d^2 \ ,$$

and

$$a_2 = -5.8 \times 10^8 + 1.8 \times 10^7 d + 8.9 \times 10^5 d^2 \ .$$

Eq. (22) is assumed valid for temperatures between 1500 and 2100 C and for grain sizes between d = 2.0 and d = 14.5 μm.

5. Comparison of code predictions for steady-state conditions with experimental results

In this section, GRASS-SST steady-state results for the irradiations of fuel used in DEH testing will be discussed. GRASS-SST results for other steady-state irradiations have been discussed previously [30].

The purpose of the steady-state simulation is to establish the initial conditions in the fuel pellet prior to DEH testing (e.g. bubble-size distributions and amounts and location of retained gas). GRASS-SST simulated a steady-state irradiation of commercial PWR fuel in the H. B. Robinson reactor and an irradiation of rod 843 in the Saxton reactor. For these steady-state irradiations,

GRASS-SST was run with an experimental version of the LIFE-LWR fuel-behavior code [41]. Table 3 shows the results of the steady-state simulations for total gas release from the rods as well as the quantity of gas retained in the pellets used for DEH testing. Also listed in table 3 are the experimentally determined values for these quantities. From table 3, the calculated quantity of retained gas in the pellets prior to DEH testing are in reasonable agreement with the data.

As an additional check that GRASS-SST is supplying the correct initial conditions to the transient analysis, the GRASS-SST-calculated intragranular bubble density versus bubble diameter at a fractional radius of $\sim$0.20 for the H. B. Robinson fuel pellets at end of life is shown in fig. 11. Also shown in fig. 11 is an estimate of the measured density of fission-gas bubbles obtained from replica fractographs (see section 2.1). Bubbles with diameters <100 Å were below the limit of resolution and thus were not observable. The calculated bubble-size distribution, shown in fig. 11, consists mainly of fission-gas atoms and quite small ($\sim$100 Å) fission-gas bubbles. The absence of large bubbles is due to the low fuel temperatures characteristic of the H. B. Robinson irradiation, especially during the second cycle when center-line temperatures were $\sim$900°C. From fig. 11, the calculated bubble densities are in reasonable agreement with the data.

6. Comparison of code predictions for transient gas release with experimental results

Fig. 12 shows the results of GRASS-SST calculations of transient gas release versus the measured results from the DEH tests shown in fig. 3 for which fuel temperature and gas-release data were available. The diagonal line indicates the position of perfect agreement between GRASS-SST predictions and experiment. The calculated results in fig. 12 were made utilizing eq. (21).

As is evident, the GRASS-SST predictions are in good agreement with the experimental measurements. Using diffusivities obtained by setting $\alpha_i = 0$ in eq. (21), i.e. using the empirical diffusivities given by eq. (19), the code significantly underpredicts the data for transient gas release >5%, except for test 31 for which the data are overpredicted by about a factor of two.

The fact that GRASS-SST can predict the DEH transient gas release for all DEH tests, including test 31, supports the hypothesis described in section 4, i.e. the mobility of fission-gas bubbles is enhanced when the bubble is overpressurized, if the equivalent stress generated as a result of the excess pressure in the bubble exceeds the yield strength of the surrounding matrix.

An additional demonstration of the need to model the effect that transient heating has on bubble mobility is given by the following example. Suppose the capability of GRASS-SST to predict DEH transient gas release depends only upon a relationship between the bubble mobilities and the transient temperature and not on other parameters such as heating rate and UO_2 yield strength. For this case, the bubble diffusivities during transient heating could be described by the curve shown in fig. 13. In fig. 13, a transition curve initiates at some critical temperature, T_c, and connects the steady-state diffusivities with those given by the theory of surface diffusion. Fig. 14 shows the results, using the bubble diffusivities shown in fig. 13, of GRASS-SST calculations of transient gas release versus the measured results for the DEH tests shown in fig. 12. Except for tests 24, 31, and 32, the GRASS-SST predictions (fig. 14) based on the diffusivities shown in fig. 13 are in reasonable agreement with much of the data. The predictions for transient gas release from tests 24, 31, and 32 are off by more than a factor of two (test 35 was not run for this case). The reason for this overprediction of transient gas release is that the diffusivities shown in fig. 13 describe enhanced diffusion of gas bubbles even during periods when the heating rate is relatively low. This relatively low rate of heating is characterized by test 31, which had a long steady-state

preheat at high power. The analysis leading to eq. (21) accounts for the dependence of bubble mobility on heating rate and, as is evident from fig. 12, predicts transient gas release in good agreement with the measured values for all the data. As other DEH test results become available, the validity of eq. (21) will continue to be examined.

7. Conclusions

The results of GRASS-SST predictions for transient fission-gas release during DEH tests are in excellent agreement with experimental data. Comparisons of GRASS-SST predictions of gas release and bubble-size distributions with the results of DEH transient tests indicate that (a) coalescing bubbles do not have sufficient time to grow to equilibrium size during most transient conditions, (b) the mobilities of fission-gas bubbles in UO_2 are enhanced during non-equilibrium conditions, if the excess pressure in the bubble is sufficient to generate an equivalent stress greater than or equal to the yield stress of the surrounding matrix, and (c) channel formation on grain surfaces and coalescence of the channels with each other and with the tunnels of gas along the grain edges can contribute to grain-boundary separation and/or the rapid, long-range interconnection of porosity. The phenomena of grain-boundary separation and/or long-range interconnection of porosity provides an important release mechanism for fission gas that has moved out of the grains of irradiated fuel.

References

[1] The Role of Fission Gas Release in Reactor Licensing, NUREG-75/077, Core Performance Branch, U.S. Nuclear Regulatory Commission, November 1975.

[2] C. E. Beyer and C. R. Hann, Prediction of Fission Gas Release from UO_2 Fuel, BNWL-1875 (1974).

[3] A. H. Booth, A Method of Calculating Fission Gas Diffusion from UO_2 Fuel, Chalk River Report, CRDC-721 (1957).

[4] W. A. Yuill, V. F. Baston and J. H. McFadden, Idaho Nuclear Report, IN-1467 (1971).

[5] J. R. MacEwan and W. H. Stevens, J. Nucl. Mater. 11 (1964) 77.

[6] R. M. Carroll, R. B. Perez and O. Sisman, J. Amer. Ceram. Soc. 48 (1965) 55.

[7] R. S. Barnes and D. J. Mazey, Electron Microscopy 1964, Proceedings of the Third European Regional Conference (Czech. Acad. Sci., Prague, 1965) p. 197.

[8] A. D. Whapham, Nucl. Appl. 2 (1966) 123.

[9] J. A. Turnbull and M. O. Tucker, Phil. Mag. 30 (1972) 47.

[10] W. B. Beere and G. L. Reynolds, J. Nucl. Mater. 47 (1973) 51.

[11] S. M. Gehl, M. G. Seitz and J. Rest, "Relationship between Fission-gas Release and Microstructural Change during Transient Heating of Pressurized Water Reactor Fuel," Proc. ANS Topical Mtg. on Thermal Reactor Safety, 1977, CONF-770708, Vol. 3, pp. 3-261 to 3-282.

[12] S. M. Gehl, M. G. Seitz and J. Rest, Argonne National Laboratory, ANL-77-80, in press (1977).

[13] R. B. Poeppel, "An Advanced Gas Release and Swelling Subroutine," Proceedings of Conference on Fast Reactor Fuel Element Technology (Am. Nucl. Soc., Hinsdale, Ill., 1971) pp. 311-326.

[14] V. Z. Jankus and R. W. Weeks, Nucl. Eng. and Design 18(1) (1972) 83-96.

[15] V. Z. Jankus, "Fast-reactor Fuel-element Analysis Using Multiregion Formulation in LIFE-II," 2nd International Conference on Structural Mechanics in Reactor Technology, Vol. VI, Part A Suppl. D2/5, Berlin, Germany (1973).

[16] S. M. Gehl, et al. in "Light-water-reactor Safety Research Program: Quarterly Progress Report, July-September 1975," ANL-75-72, pp. 42-3.

[17] R. A. Lorenz, J. L. Collins and S. R. Manning, "Quarterly Progress Report on Fission Product Release from LWR Fuel for the Period Oct.-Dec. 1975," ORNL/TM-5290 (March 1976).

[18] G. W. Gibson, et al., ANCR-NUREG-1321 (1976).

[19] D. Freund and W. Schikarski, KFK-1031, EURFNR-773 (1970).

[20] B. J. Wrona and E. Johanson, Nucl. Technol., 29 (1976) 433.

[21] J. C. Voglewede, Argonne National Laboratory, private communication.

[22] A. B. G. Washington, "Preferred Values for Thermal Conductivity of Sintered Ceramic Fuel for Fast Reactor Use," UKAEA TRG-Report-2236 (September 1973).

[23] F. Forscher, J. Franklin Inst., 259 (1955) 107-14.

[24] T. H. Blakely and A. E. S. White, in Plansee Proc. 2nd Seminar, Routte/ Tyrol. ed. by F. Benesousky (Pergamon Press, London, 1956) pp. 335-45.

[25] J. Gurland, Trans. Met. Soc. AIME, 236 (1966) 642-46.

[26] A. S. Mehner, W. J. Quapp, R. R. Hobbins, S. L. Seiffert and R. K. McCardell, "Performance of Unirradiated and Irradiated PWR Fuel Rods Tested under Power-Cooling-Mismatch Conditions," Proc. ANS Topical Mtg. on Thermal Reactor Safety, 1977, CONF-770708, Vol. 3, pp. 3-1 to 3-28.

[27] W. L. Wang and R. N. Singh, "Relaxation Theory of Nonequilibrium Fission-gas Bubbles and Criteria for Equilibrium," submitted to the J. Nucl. Mater. (1977).

[28] G. Bandyopadhyay, "Fuel and Fission-gas Response to Simulated Thermal Transients: Experimental Results and Correlation with Fission-gas Release and Swelling Model," submitted to the J. Nucl. Tech. (1977).

[29] M. W. Finnis, M. R. Hayns and R. Bullough, AERE-R-7970 (1975).

[30] J. Rest, M. G. Seitz, S. M. Gehl and L. R. Kelman, "Development and Experimental Verification of SST-GRASS: A Steady-state and Transient Fuel Response and Fission-product Release Code," Proc. of the CSNI Specialists Meeting on the Behavior of Water Reactor Fuel Elements under Accident Conditions, Spatind, Norway, Sept. 13-16, 1976.

[31] M. G. Seitz, S. J. Gehl and C. H. Gebo, "Light Water Reactor Safety Research Program: Quarterly Progress Report," April-June 1976, ANL-76-87 (1976) pp. 20-24.

[32] J. C. Fisher, J. Appl. Phys. 22 (1974) 74-77.

[33] K. Maschke, H. Overhof and P. Thomas, Phys. Stat. Sol. (b) 60 (1973) 563.

[34] L. E. Willertz and P. G. Shewmon, Met. Trans., 1 (1970) 2217-2223.

[35] W. Oldfield and J. B. Brown, Jr., Mater. Sci. Eng., 6 (1970) 361-370.

[36] W. Beere, J. Nucl. Mater. 45 (1973) 91-95.

[37] W. Beere and G. L. Reynolds, Acta Metall., 20 (1972) 845-858.

[38] C. Baker, J. Nucl. Mater., 71 (1977) 117-123.

[39] W. B. Beere, Phil. Mag. 25 (1972) 189-200.

[40] J. T. A. Roberts, Deformation of Ceramic Materials, eds., R. C. Bradt and R. E. Tressler (Plenum Press, New York, 1975) p. 325.

[41] J. Rest, M. C. Billone and V. Z. Jankus, "Light Water Reactor Safety Research Program: Quarterly Progress Report," July-September 1976, ANL-76-121 (1976) pp. 50-61.

List of Figures

Table 1

Postirradiation fission-gas retention for Robinson and Saxton fuels

Fuel type	Gas retention (μmole/gUO_2)	
	Xe	Kr
Robinson	30.6	2.4
Saxton	16	2

Table 2

Experimental data for DEH tests

Test no.	Test duration (s)	Avg. power ramp rate, (W/s)	Energy input (10^4 W·s)	Xe release (μmole/g)	Xe release (%)	Kr release (μmole/g)	Kr release (%)	Fractional melt radius	Gas release from unmelted fuel (%)[a] Xe	Gas release from unmelted fuel (%)[a] Kr	Avg. center heating rate (°C/s)	Max. center temp. (°C)	Swelling (%)	$S_g^{\alpha P}$ (10^4 mm^2/g)
21	68	10	3.16	14.3 ± 0.3	50.0 ± 1.0	1.3	60	0.33	44.1	55	NA[c]	NA	25.0	4.12
22	36	7.3	1.64	3.8 ± 0.1	13.1 ± 0.5	0.54	25				35	2480	14.8	2.93
23	28	7.3	1.17	0.3-1.3	1-5	0.04-0.2	2-10				28	1970	NA	NA
24	50	8.4	2.54	3.7 ± 0.1	12.0 ± 0.5	0.71	30				25	2610	12.4	2.10
26	54	2.1	4.32	19.1 ± 0.5	63.1 ± 1.6	1.4	61	0.32	59 ± 2	57	<36	<3420	31.8	4.69
27	54	7.4	3.24	10.0 ± 0.2	33.3 ± 0.7	1.5	63				24	2850	NA	NA
29	59	4.5	2.50	0.62 ± 0.2	2.0 ± 0.6	0.09	4				7.6	1560	0	0
30	70	0.7	1.46	0.1 ± 0.03	0.4 ± 0.1	0.02	0.8				6.0	1280	NA	NA
31	71	12	62.7	6.3 ± 0.5	20.1 ± 1.5	0.45	19				12	2850	11.1	2.54
32	60	5.5	2.59	4.9 ± 0.7	16.1 ± 2.4	0.36	15				20	2600	18.1	2.68
33	100	5.0	4.14	13.0 ± 0.7	42.6 ± 2.2	1.2	49	0.20	40 ± 2.6	47	15	2950	23.3	4.23
35[b]	37	16	1.92	2.2 ± 0.4	16 ± 2.9	0.42	17	0.20	12 ± 2.2	14	45	3010	NA	NA
36	11	100	0.96	7.0 ± 0.9	22.8 ± 3.0	0.47	20				76	2520	NA	NA

[a]Assuming that all gas was released from the fuel that melted.

[b]Saxton fuel.

[c]NA = not available.

Table 3

GRASS-SST calculated values for total gas release from Saxton and H. B. Robinson fuel rods and for the quantity of gas retained in pellets used for DEH testing compared with experimental results

Fuel	Total calculated gas release from rod (mm mole)	Total measured gas release from rod (mm mole)	Total calculated quantity of gas remaining in fuel pellet (μmole/g)	Total measured quantity of gas remaining in fuel pellet (μmole/g)
H. B. Robinson	0.12	0.18	36	31
Saxton	1.15	0.958	17	16

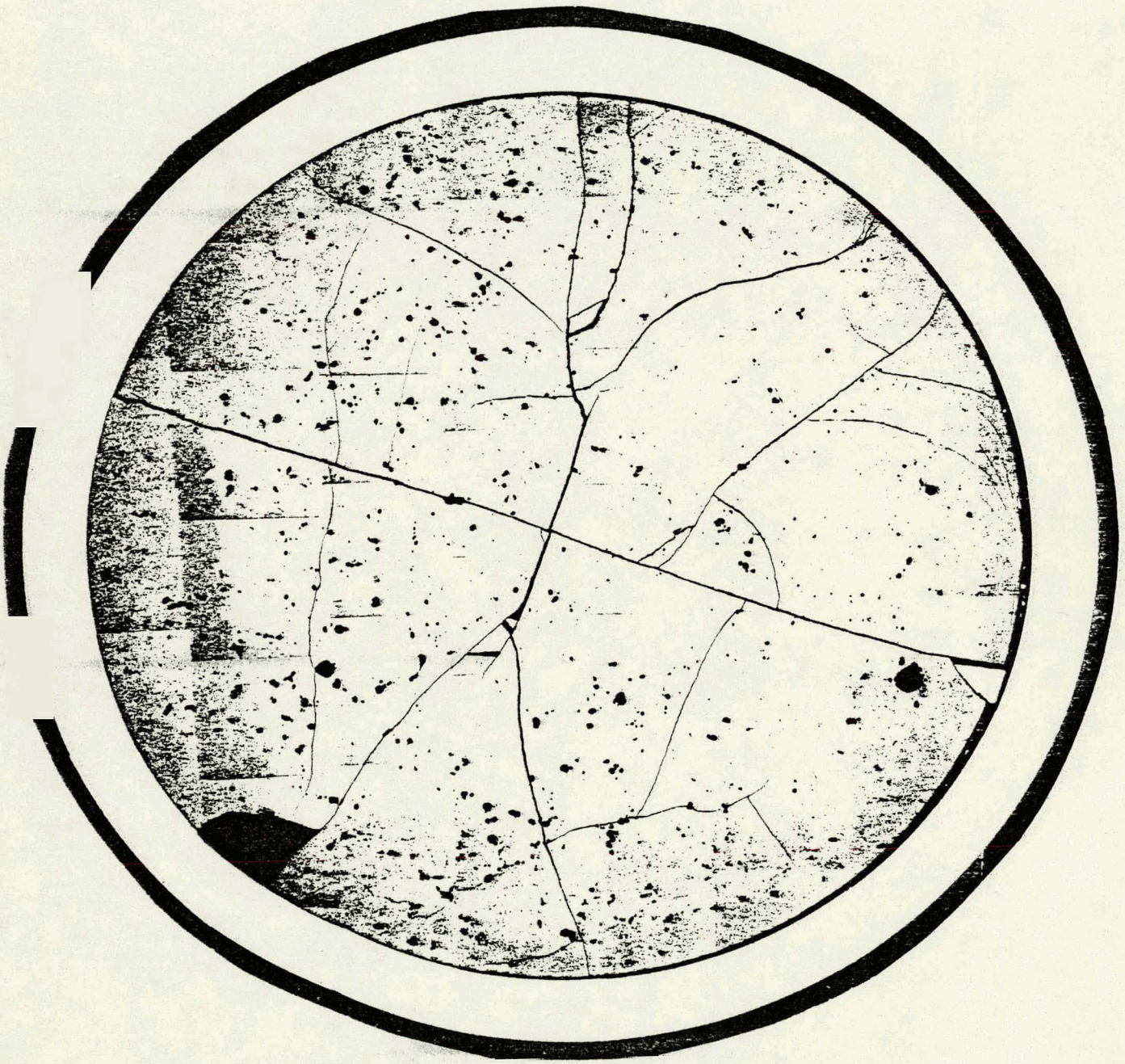

Fig. 1. Transverse section through the high power region of Robinson rod F7.

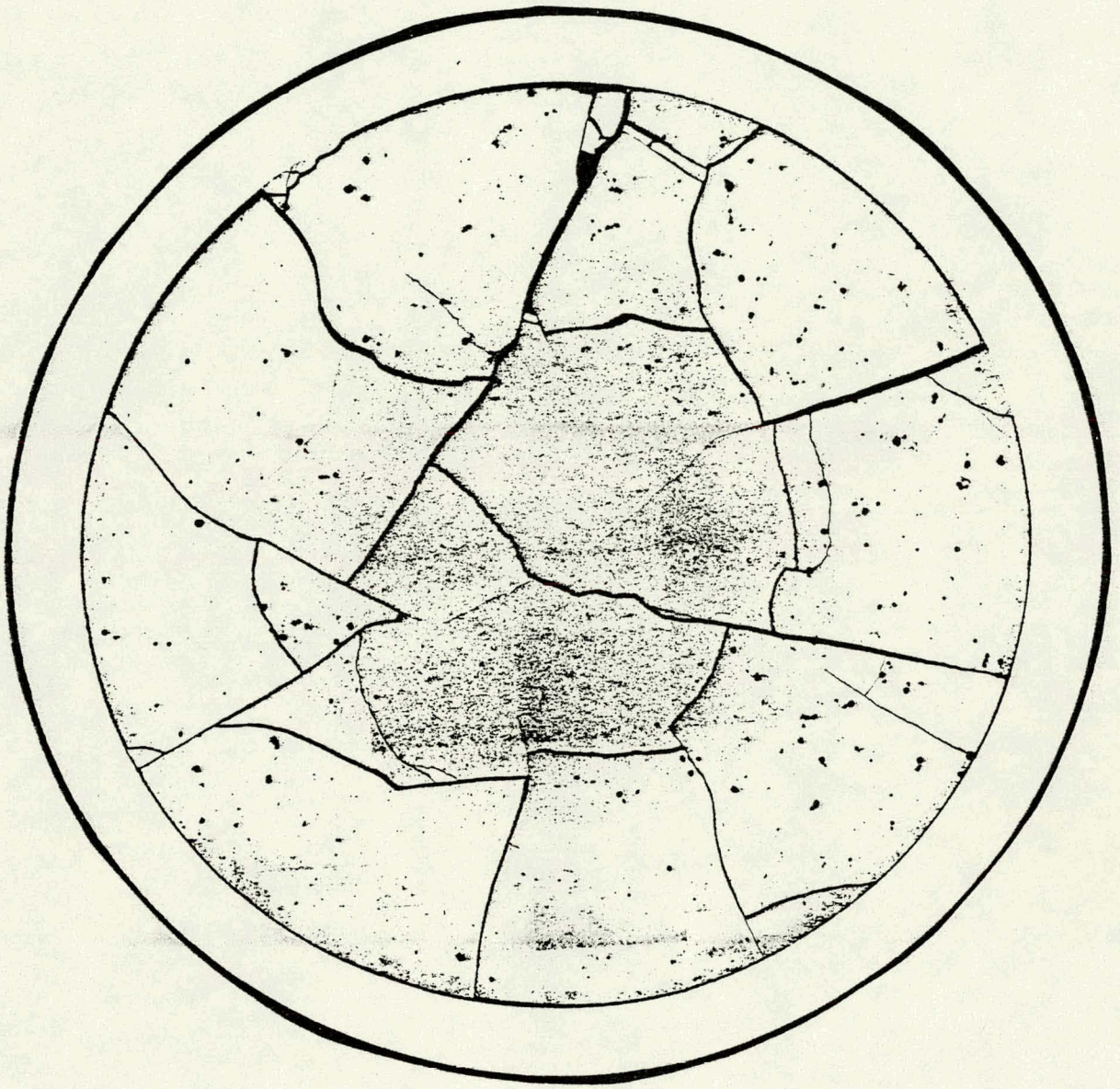

Fig. 2. Transverse section through Saxton rod 843 near the peak power position.

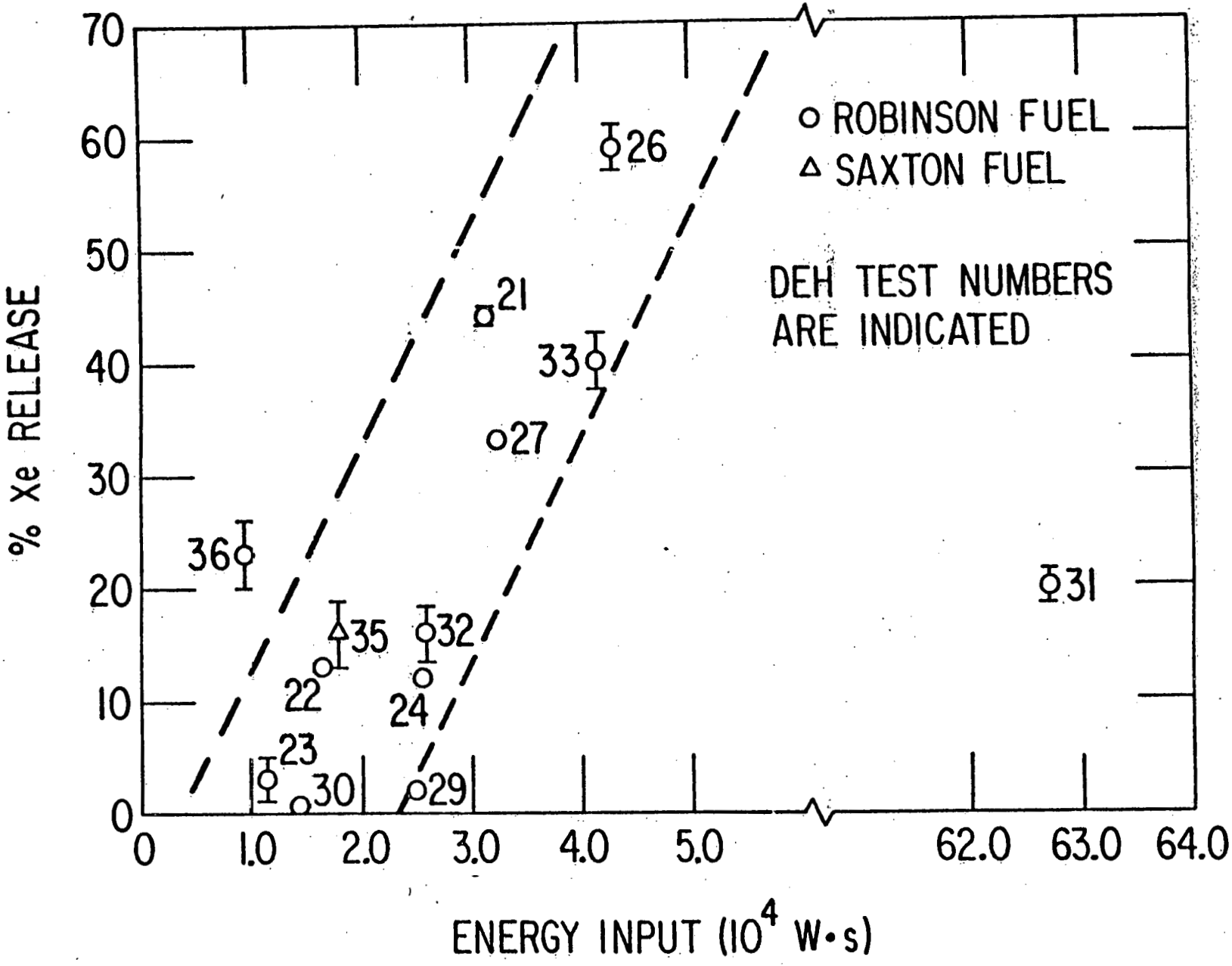

Fig. 3. Percent Xe release vs energy input for DEH-tested specimens.

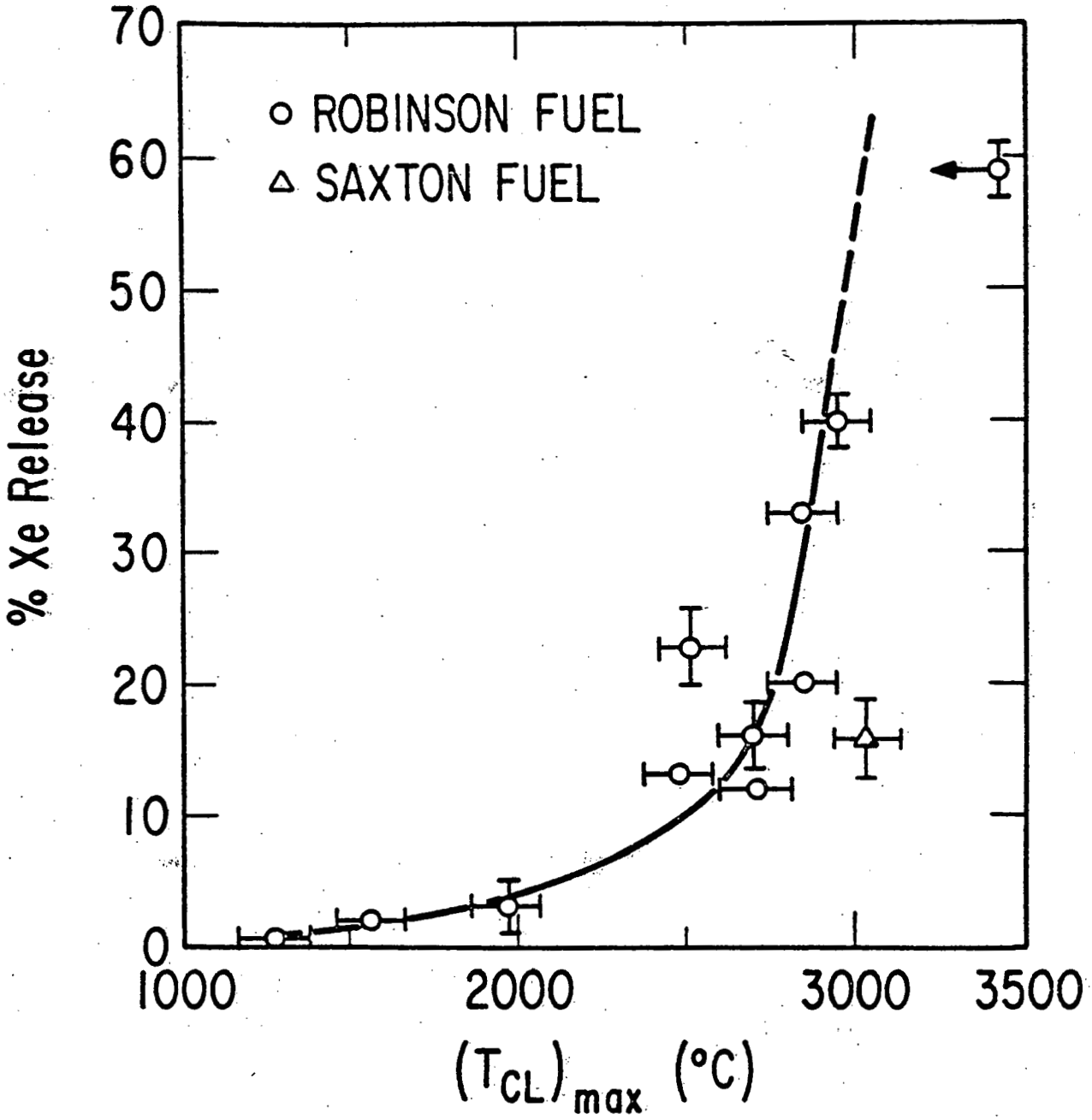

Percent Xe Release as a Function of Maximum Centerline Temperature

Fig. 4. Percent Xe release vs maximum center temperature during DEH testing.

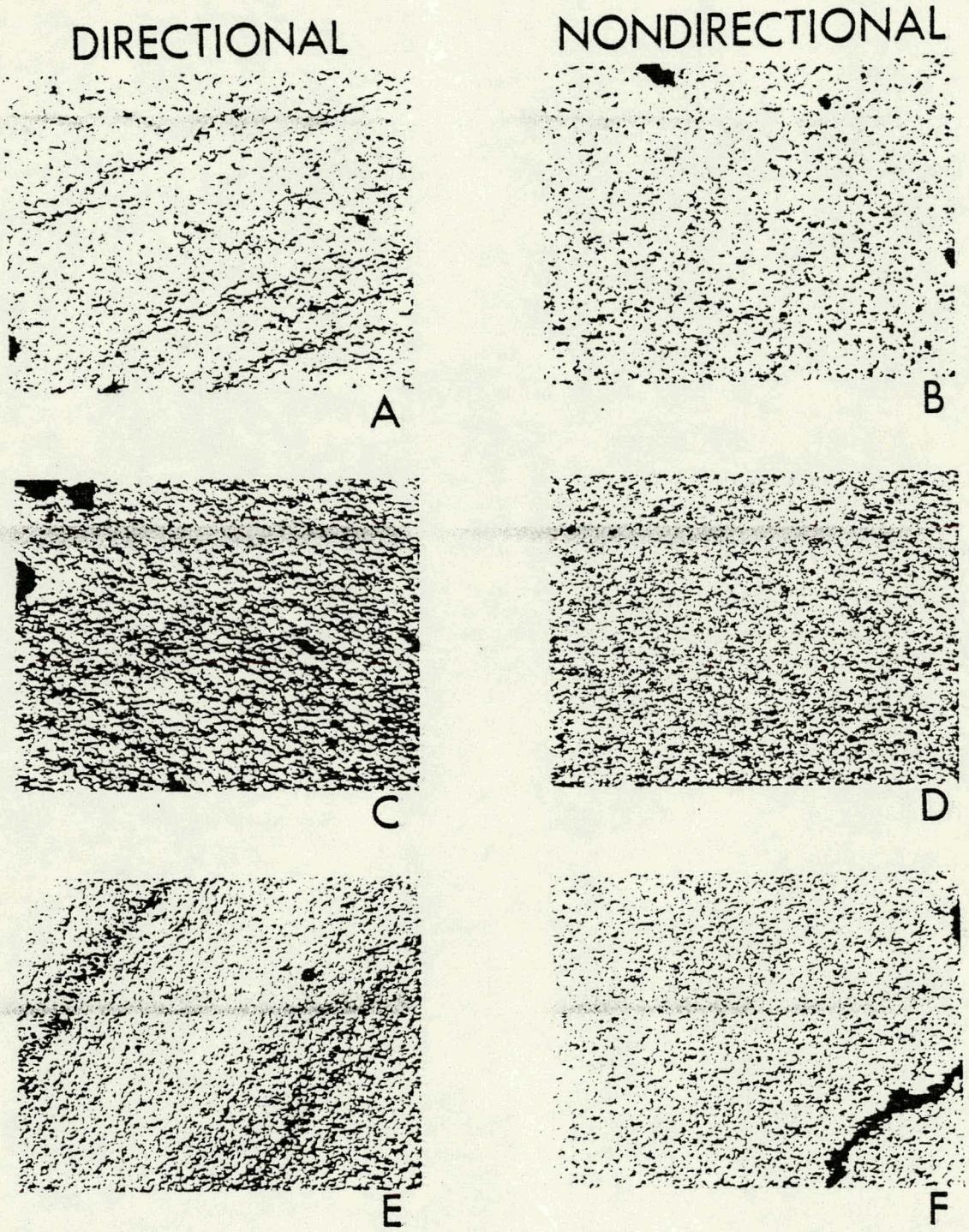

Fig. 5. Optical micrographs of intergranular separations in DEH-tested fuel.

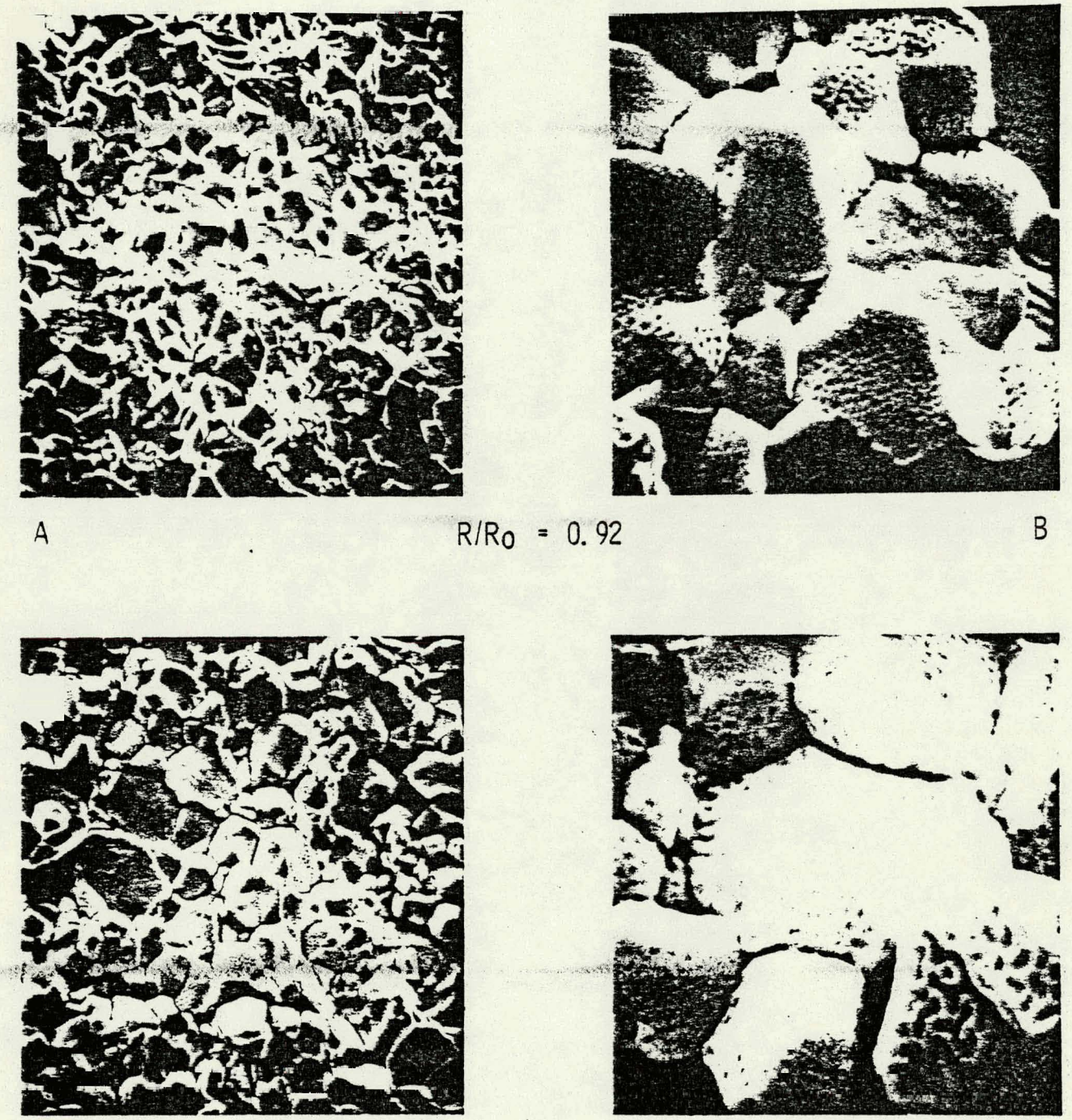

Fig. 6. Scanning electron fractographs at four radial positions in a Robinson fuel pellet after DEH test 24.

E

F

$R/R_0 = 0.75$

20 μm

$R/R_0 = 0.53$

G

2 μm

Fig. 6. (Contd.)

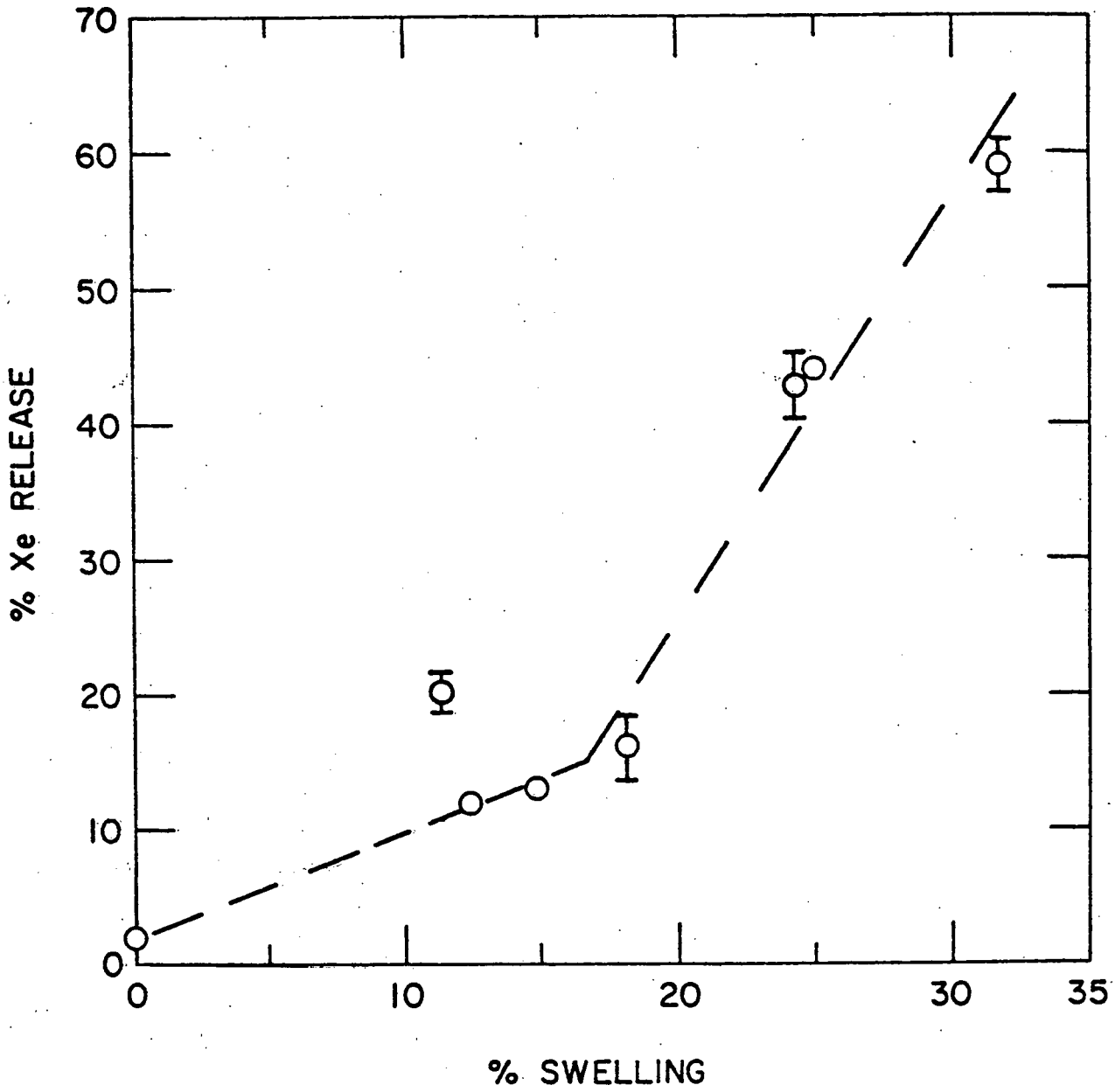

Percent Xe Release as a Function of Volume-averaged Swelling

Fig. 7. Percent Xe release vs volume-averaged swelling.

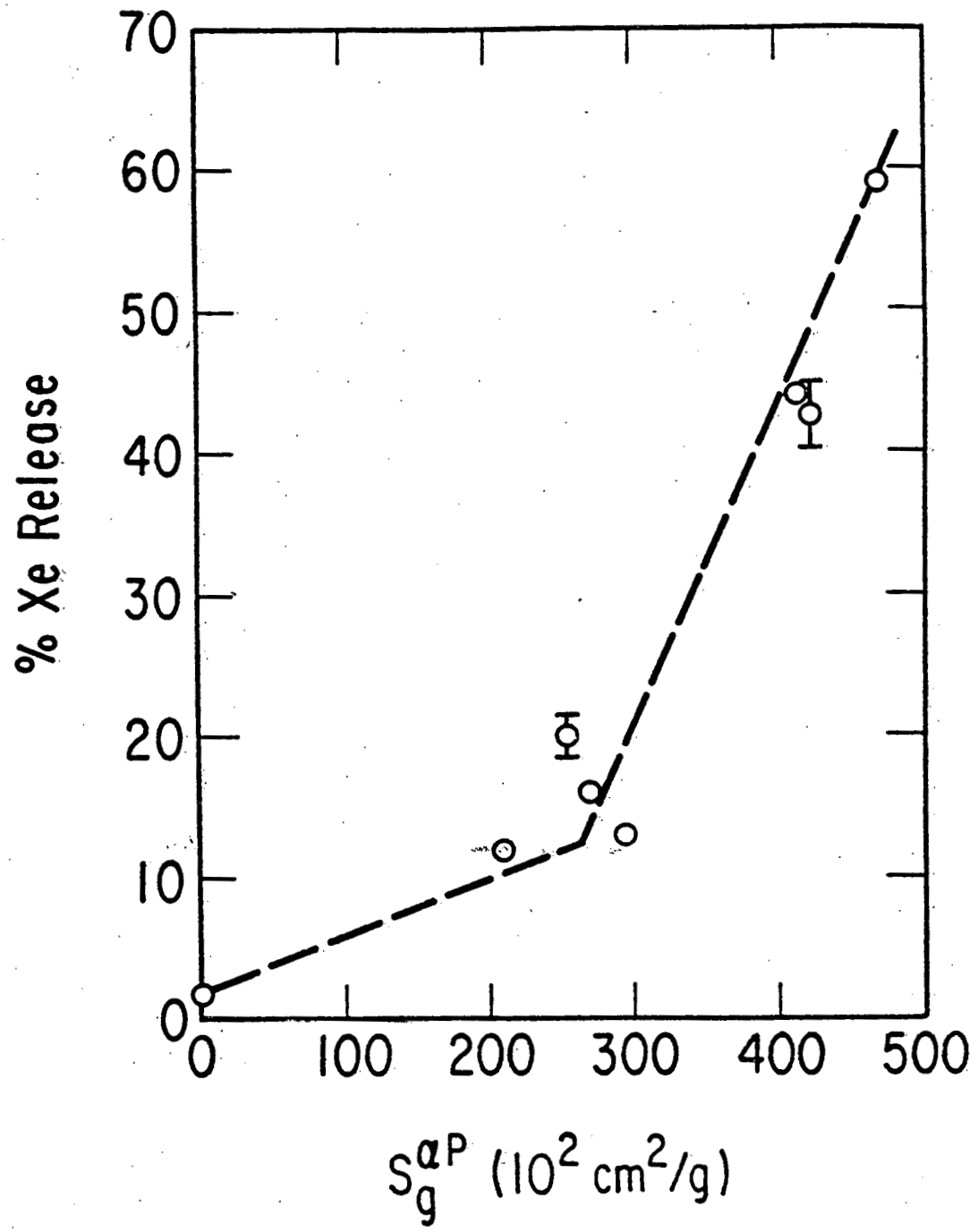

Percent Xe Release as a Function of New Pore-Solid Surface Area

Fig. 8. Percent Xe release vs new pore-solid surface area.

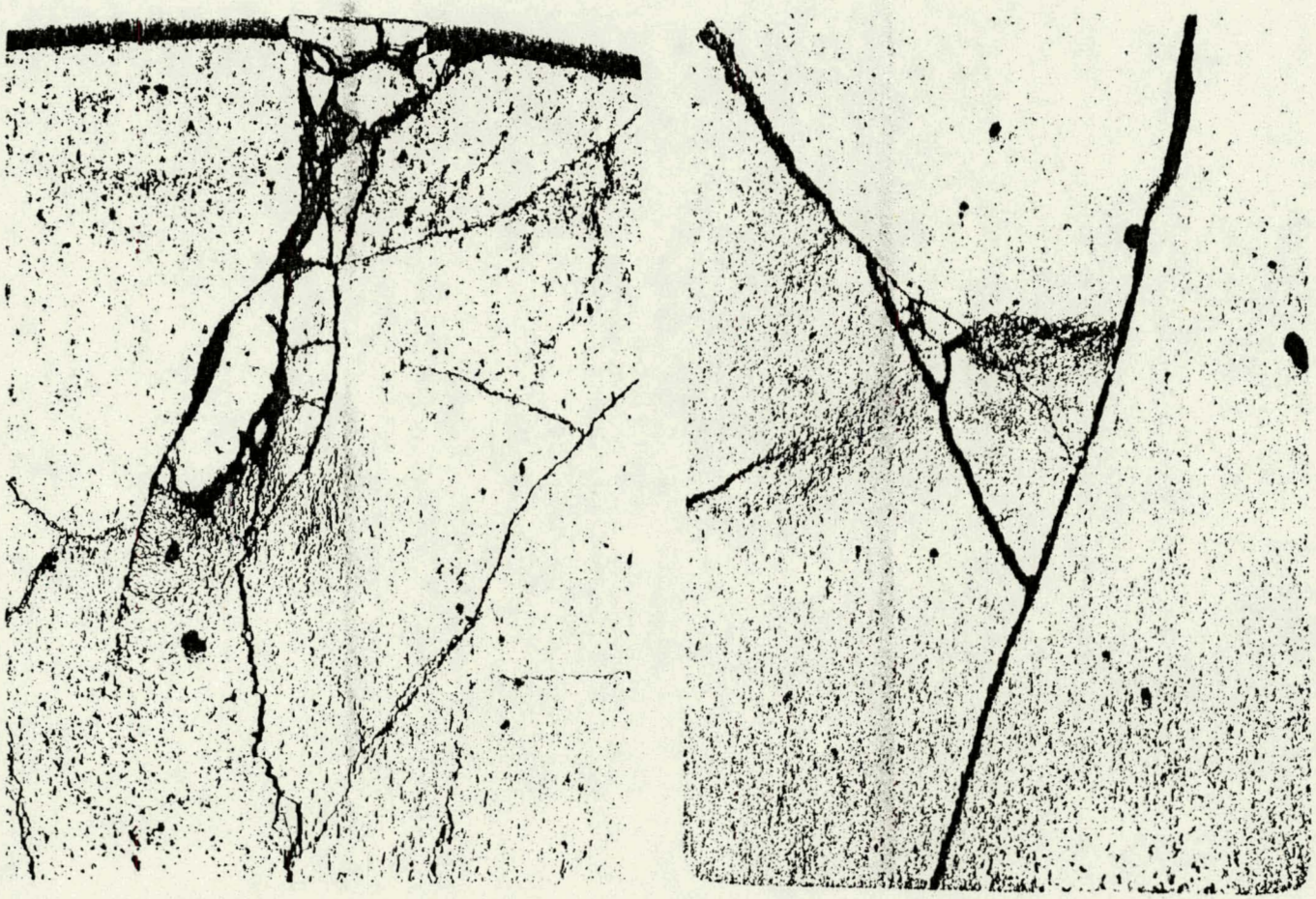

Fig. 9. Intergranular separations in (A) PBF- and (B) DEH-tested fuel.

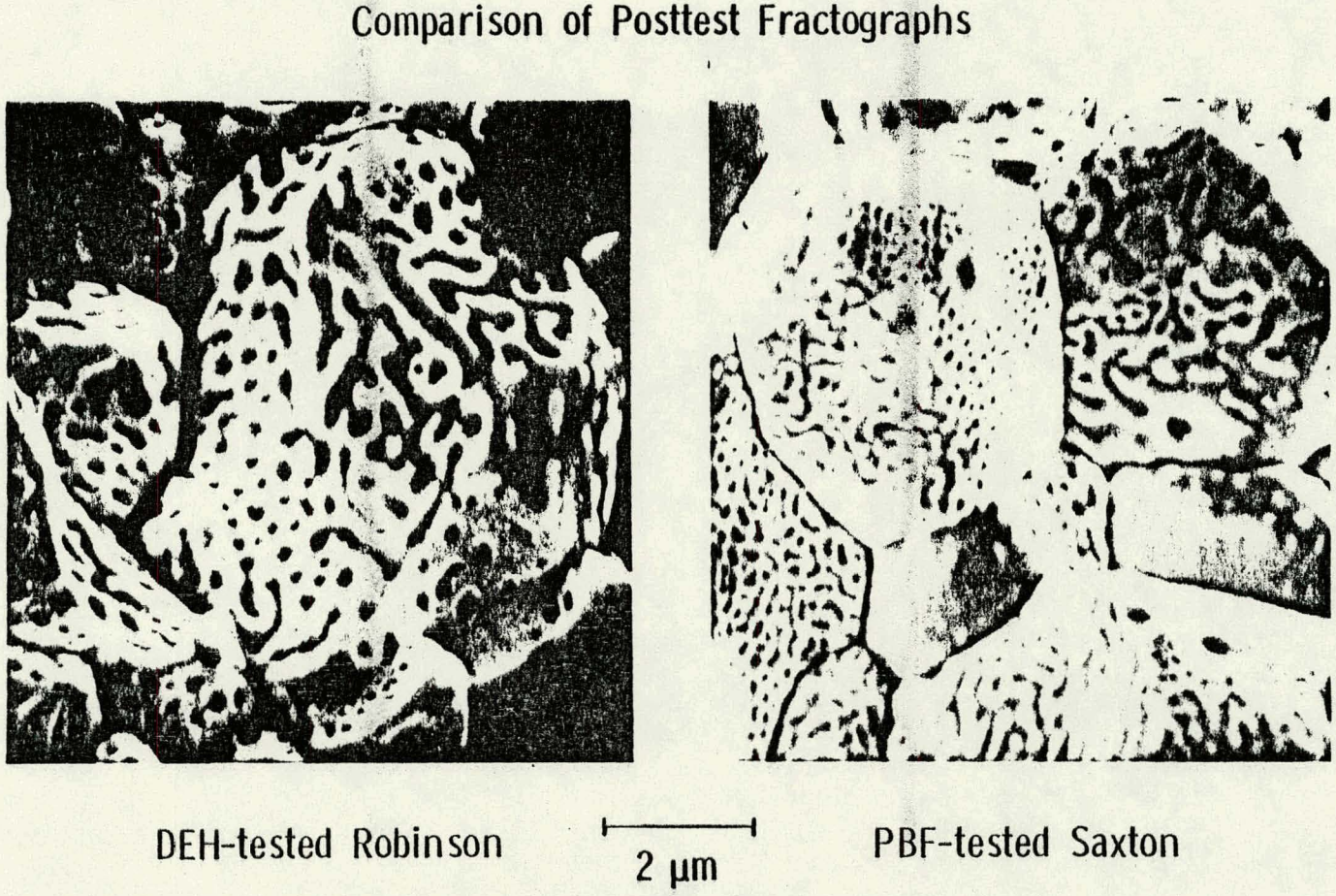

Fig. 10. SEM fractographs of Robinson and Saxton fuels.

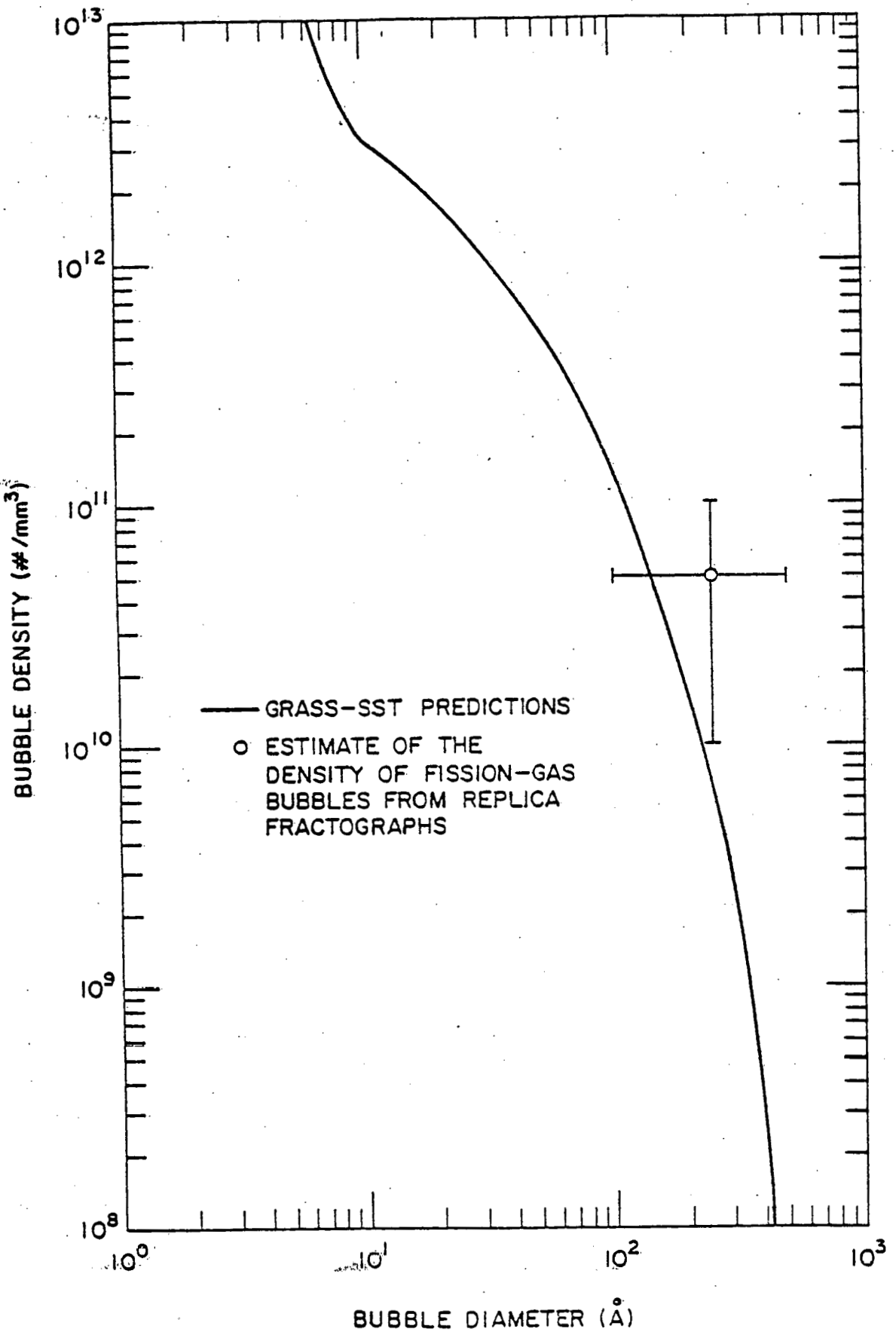

Fig. 11. GRASS-SST calculated intragranular bubble density vs bubble diameter for H. B. Robinson fuel at end of life compared with experimental data. Bubbles with diameters ≲100 Å were below the limit of resolution.

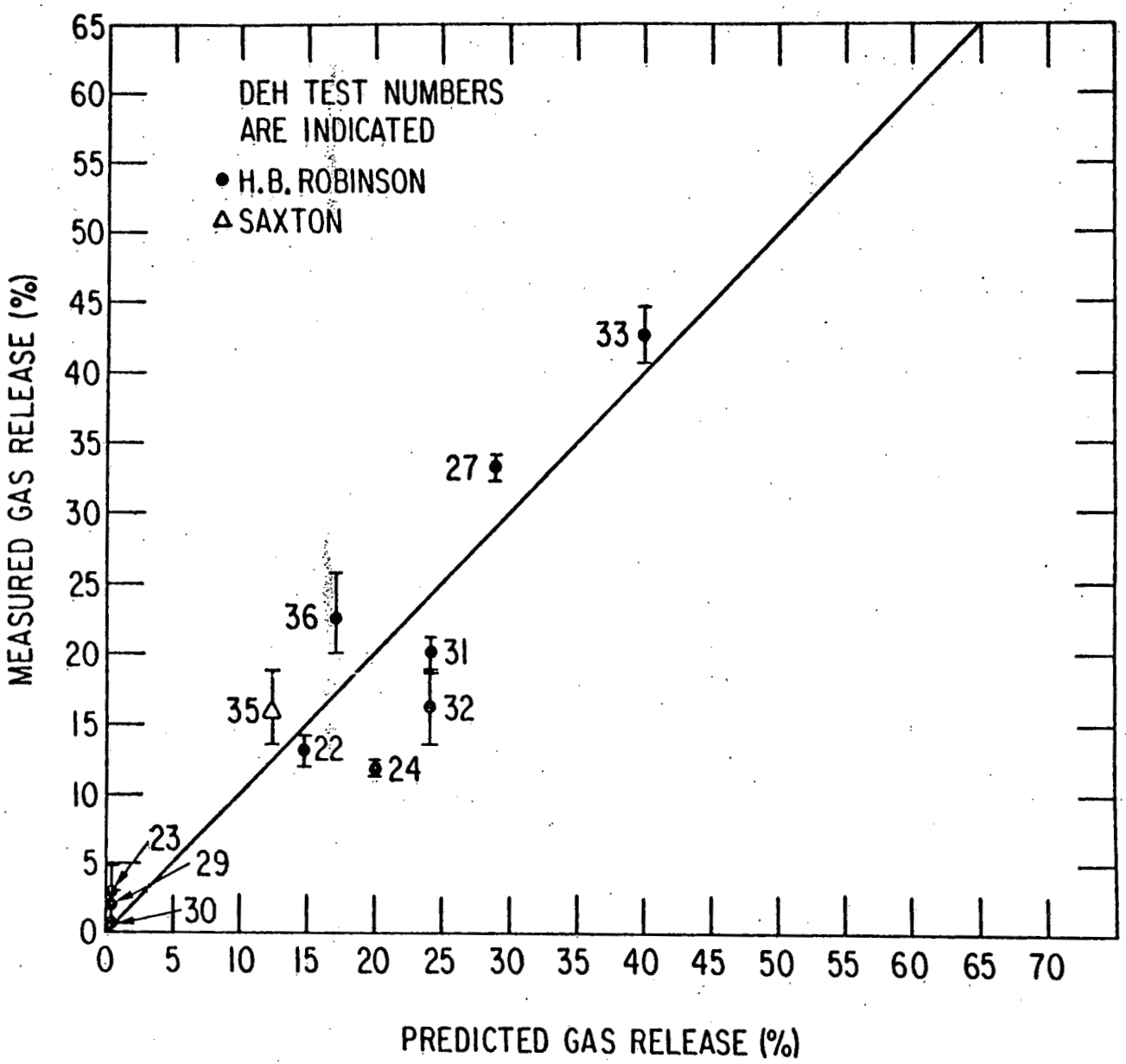

Fig. 12. GRASS-SST-predicted transient gas release using eq. (21) vs experimentally measured values.

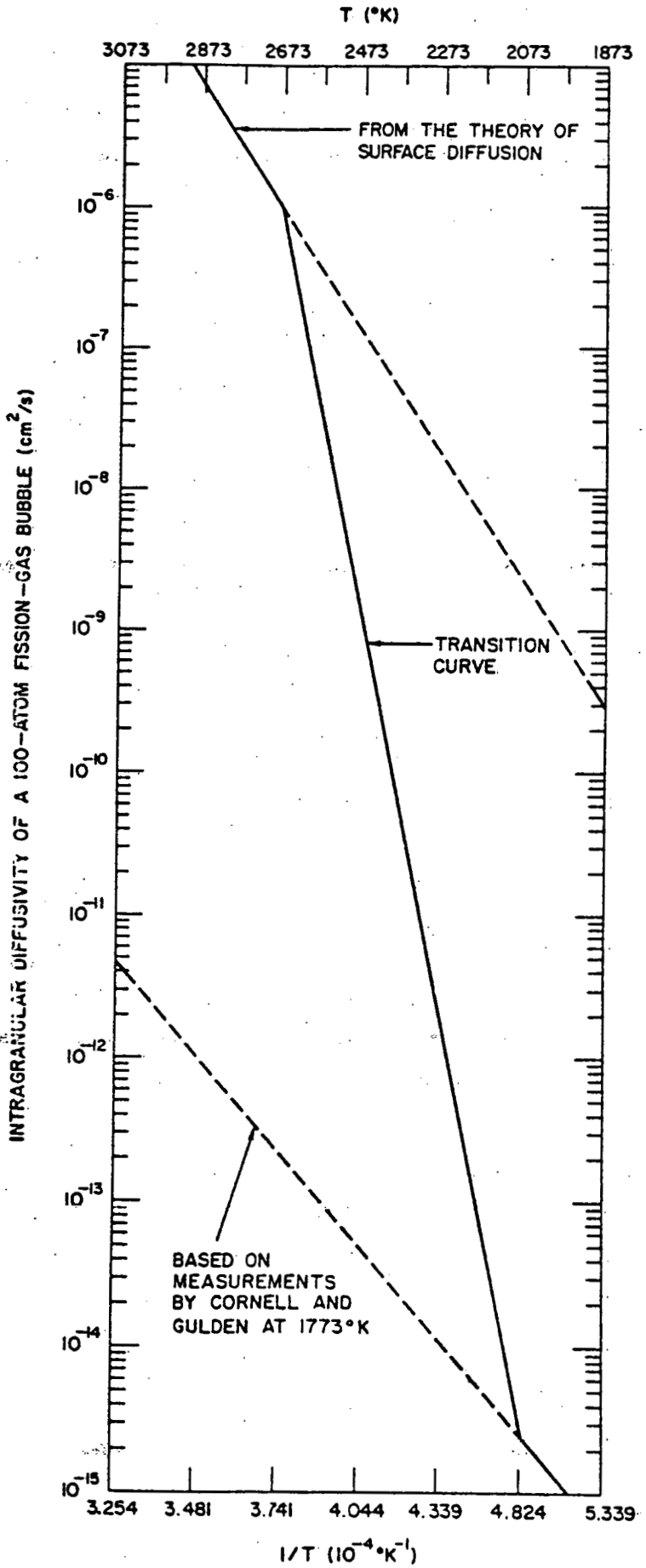

Fig. 13. Intragranular diffusivity of a 100-atom fission-gas bubble as a function of 1/T, assuming a temperature-dependent transition curve.

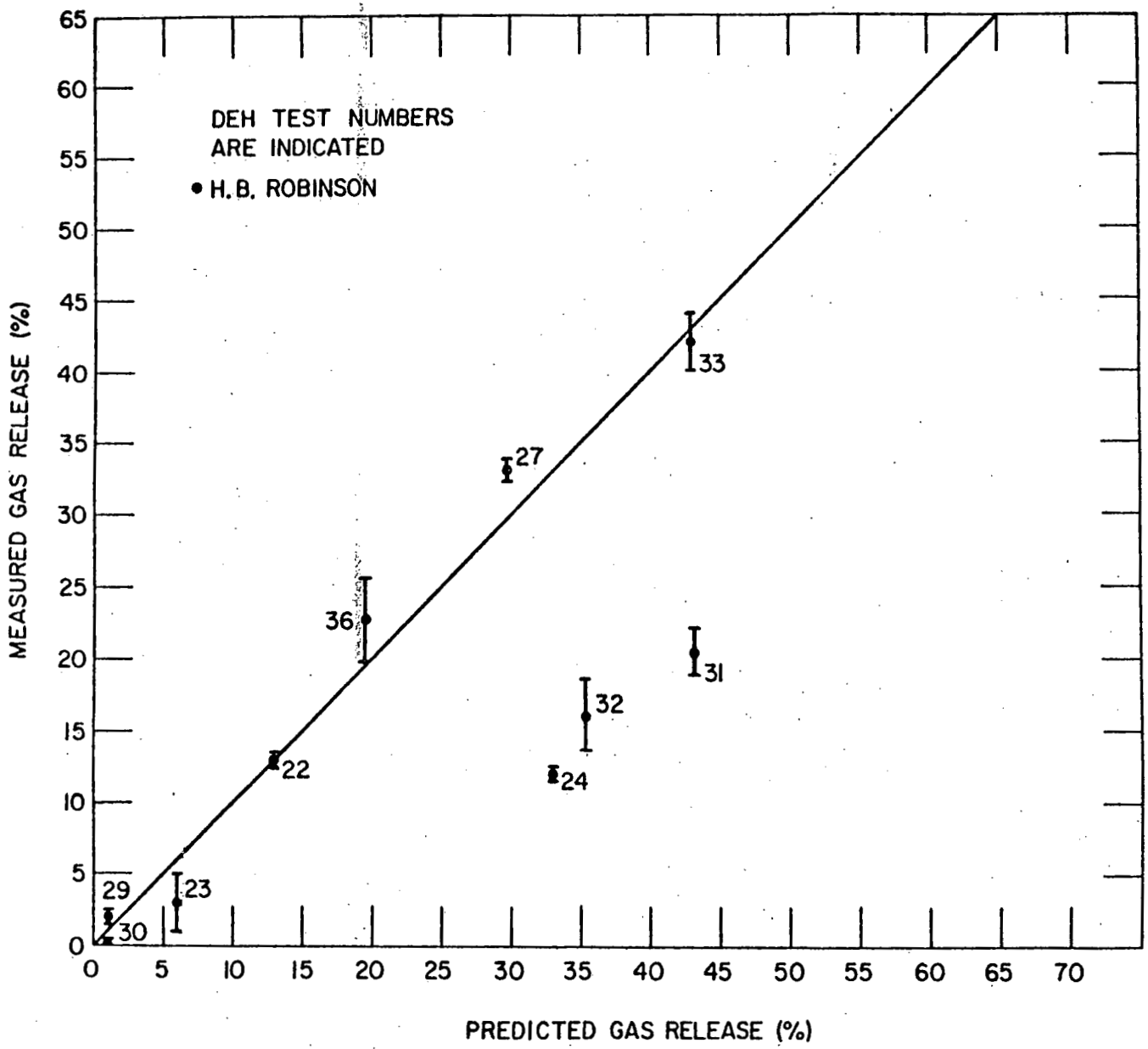

Fig. 14. GRASS-SST-predicted transient gas release using the assumed temperature-dependent diffusivities shown in fig. 13 vs experimentally measured values. These results indicate the need for a dependence of heating rate on gas-bubble diffusivity, e.g. as described by eq. (21) and discussed in the text.